

# Molecular basis of the PIP<sub>2</sub>-dependent regulation of Ca<sub>v</sub>2.2 channel and its modulation by Ca<sub>v</sub> β subunits

Cheon-Gyu Park, Wookyung Yu, Byung-Chang Suh\*

Department of Brain Sciences, Daegu Gyeongbuk Institute of Science and Technology (DGIST), Daegu, Republic of Korea

**Abstract** High-voltage-activated Ca<sup>2+</sup> (Ca<sub>v</sub>) channels that adjust Ca<sup>2+</sup> influx upon membrane depolarization are differentially regulated by phosphatidylinositol 4,5-bisphosphate (PIP<sub>2</sub>) in an auxiliary Ca<sub>v</sub> β subunit-dependent manner. However, the molecular mechanism by which the β subunits control the PIP<sub>2</sub> sensitivity of Ca<sub>v</sub> channels remains unclear. By engineering various α1B and β constructs in tsA-201 cells, we reported that at least two PIP<sub>2</sub>-binding sites, including the polybasic residues at the C-terminal end of I-II loop and the binding pocket in S4<sub>II</sub> domain, exist in the Ca<sub>v</sub>2.2 channels. Moreover, they were distinctly engaged in the regulation of channel gating depending on the coupled Ca<sub>v</sub> β2 subunits. The membrane-anchored β subunit abolished the PIP<sub>2</sub> interaction of the phospholipid-binding site in the I-II loop, leading to lower PIP<sub>2</sub> sensitivity of Ca<sub>v</sub>2.2 channels. By contrast, PIP<sub>2</sub> interacted with the basic residues in the S4<sub>II</sub> domain of Ca<sub>v</sub>2.2 channels regardless of β2 isotype. Our data demonstrated that the anchoring properties of Ca<sub>v</sub> β2 subunits to the plasma membrane determine the biophysical states of Ca<sub>v</sub>2.2 channels by regulating PIP<sub>2</sub> coupling to the nonspecific phospholipid-binding site in the I-II loop.

## Editor's evaluation

This manuscript describes experiments using heterologous expression to achieve molecular dissection of the effects of PIP<sub>2</sub> and Ca<sub>v</sub>β2 auxiliary subunits on Ca<sub>v</sub>2.1 (P/Q-type) calcium channels. The experiments also probe interplay between lipid effects and other modulatory pathways. Understanding the functional regulation of this channel is important because Ca<sub>v</sub>2.1 channels play significant roles in neuronal plasticity.

\*For correspondence:  
bcsuh@dgist.ac.kr

**Competing interest:** The authors declare that no competing interests exist.

**Funding:** See page 20

**Received:** 16 April 2021

**Accepted:** 25 October 2022

**Published:** 14 November 2022

**Reviewing Editor:** Kurt Beam, University of Colorado Anschutz Medical Campus, United States

© Copyright Park et al. This article is distributed under the terms of the [Creative Commons Attribution License](https://creativecommons.org/licenses/by/4.0/), which permits unrestricted use and redistribution provided that the original author and source are credited.

## Introduction

Voltage-gated Ca<sup>2+</sup> (Ca<sub>v</sub>) channels that mediate Ca<sup>2+</sup> influx upon membrane depolarization contribute to various physiological events, including synaptic transmission, hormone secretion, excitation–contraction coupling, and gene transcription (*Berridge et al., 2000; Catterall, 2011; Clapham, 2007; Li et al., 2016*). Ca<sub>v</sub> channels can be divided into high-voltage-activated (HVA) and low-voltage-activated (LVA) channels based on their activation voltage threshold. The HVA Ca<sup>2+</sup> channels, which consist of the Ca<sub>v</sub>1 and Ca<sub>v</sub>2 families, are multiprotein complexes with a pore-forming α1 subunit and auxiliary α2δ and β subunits. Diverse cellular factors regulate Ca<sub>v</sub> channel activity (*Felix, 2005; Huang and Zamponi, 2017*).

Among the various intracellular regulatory signals of Ca<sub>v</sub> channels, we focus on the membrane phospholipid phosphatidylinositol 4,5-bisphosphate (PIP<sub>2</sub>). Previous studies have shown that PIP<sub>2</sub> activates several types of HVA Ca<sub>v</sub> channels in recombinant systems and native tissue cells (*Hille et al., 2015; Rodríguez-Menchaca et al., 2012; Suh and Hille, 2008; Wu et al., 2002; Xie et al., 2016*).

Dr-VSP, a voltage-sensing lipid phosphatase from zebrafish, can be used to examine the effects of PIP<sub>2</sub> on Ca<sub>v</sub> channels without the involvement of other downstream second messengers generated from G<sub>q</sub>-coupled receptors (Murata et al., 2005; Okamura et al., 2009; Suh et al., 2010). In vitro experiments using Dr-VSP have shown that most HVA Ca<sup>2+</sup> channels are suppressed by membrane PIP<sub>2</sub> depletion without influencing LVA Ca<sup>2+</sup> channels (Jeong et al., 2016; Suh et al., 2010). PIP<sub>2</sub> induces two distinct and opposing regulatory effects on Ca<sub>v</sub>2.1 channels (Wu et al., 2002). Thus, the Ca<sub>v</sub>2.1 channel protein was suggested to contain two distinct PIP<sub>2</sub>-interaction sites with different binding affinity (Wu et al., 2002). A more recent study showed that four arginine residues within the C-terminal end of the I-II loop of L-type Ca<sub>v</sub>1.2 channels are involved in nonspecific phospholipid interactions; therefore, the substitution of these basic residues for alanine decreases current inhibition via PIP<sub>2</sub> breakdown and increases the open probability of Ca<sub>v</sub>1.2 channels (Kaur et al., 2015). The precise PIP<sub>2</sub>-binding sites have not been fully determined in Ca<sub>v</sub> channels yet.

Among the auxiliary subunits, Ca<sub>v</sub> β subunits directly bind to an α-interacting domain (AID) within the N-terminal region of the I-II loop. They play key roles in regulating membrane trafficking and fine-tuning the gating of Ca<sub>v</sub> channels (Buraei and Yang, 2010; Buraei and Yang, 2013). A single β subunit can be divided into five distinct regions: conserved src homology-3 (SH3) and guanylate kinase (GK) domains, a flexible HOOK region connecting the two domains, and variable N- and C-terminus. The GK domain contains an α-binding pocket (ABP), which is a site for interaction with the AID of the I-II loop (Buraei and Yang, 2010; Buraei and Yang, 2013; Chen et al., 2004; Opatowsky et al., 2004; Van Petegem et al., 2004). Additionally, the HOOK region, a flexible linker composed of around 70 amino acids, is important in determining the inactivation kinetics, current density, and PIP<sub>2</sub> regulation of Ca<sub>v</sub>2.2 channels via electrostatic interaction with the plasma membrane (PM) (Miranda-Laferte et al., 2012; Park et al., 2017; Park and Suh, 2017; Richards et al., 2007). Several studies have shown that subcellular localization of the β subunits is primarily involved in the modulation of Ca<sub>v</sub> channel gating, including inactivation kinetics, current density, and PIP<sub>2</sub> sensitivity (Keum et al., 2014; Kim et al., 2015a, Kim et al., 2016; Suh et al., 2012; Takahashi et al., 2003). For example, N-type Ca<sub>v</sub>2.2 channels coexpressed with membrane-anchored β subunits, such as β2a or β2e, show relatively slower inactivation kinetics, higher current density, and lower PIP<sub>2</sub> sensitivity than channels with the cytosolic β subunit, such as β2b, β2c, or β3 (Keum et al., 2014; Kim et al., 2015a, Kim et al., 2015b; Kim et al., 2016; Suh et al., 2012). However, the underlying mechanisms for the differential regulation of Ca<sub>v</sub>2.2 channel gating depending on the subcellular localization of Ca<sub>v</sub> β subunits has not been clearly resolved.

Previous studies have proposed a bidentate model where two palmitoyl chains of the Ca<sub>v</sub> β2a subunit compete with the interaction of the two fatty acyl chains of PIP<sub>2</sub>. Subsequently, this dislodges the PIP<sub>2</sub> molecule from its binding site on the N-type Ca<sub>v</sub>2.2 channels, decreasing the requirement for PIP<sub>2</sub> (Heneghan et al., 2009; Hille et al., 2015; Mitra-Ganguli et al., 2009; Roberts-Crowley and Rittenhouse, 2009). Using cryo-electron microscopy (cryo-EM), Dong et al., 2021 and Gao et al., 2021 have recently shown that human Ca<sub>v</sub>2.2 channels possess a PIP<sub>2</sub>-binding pocket within the S4<sub>II</sub> domain of α1B subunit. PIP<sub>2</sub> interaction to this site is required for a minor shift of the S4<sub>II</sub> domain to the I-II loop. The functional role of the PIP<sub>2</sub>-binding site in Ca<sub>v</sub>2.2 channel gating and the modulatory effects of Ca<sub>v</sub> β subunits on the PIP<sub>2</sub> interaction are yet to be defined. In this study, we developed diverse engineered α1B and β constructs and found that the Ca<sub>v</sub>2.2 channels were regulated by PIP<sub>2</sub> through at least two distinct interacting sites, including a nonspecific phospholipid-binding motif in the distal I-II loop and the binding pocket in the S4<sub>II</sub> domain. Our results revealed that the PM-anchored β2a subunit selectively disrupted PIP<sub>2</sub> interaction with the phospholipid-binding site in the I-II loop, leading to a channel state less sensitive to Dr-VSP-induced PIP<sub>2</sub> depletion. However, the S4<sub>II</sub>-binding pocket of Ca<sub>v</sub>2.2 channels interacted with PIP<sub>2</sub> regardless of the coupled β2 isotype. The present study provides new insights into the reciprocal roles of the Ca<sub>v</sub> β subunits and membrane PIP<sub>2</sub> in HVA Ca<sub>v</sub> channel regulation.

## Results

### N-terminal length of PM-tethering Ca<sub>v</sub> β subunit is important in determining current inactivation and PIP<sub>2</sub> sensitivity of Ca<sub>v</sub>2.2 channels

We have previously reported that subcellular localization of the Ca<sub>v</sub> β subunit plays an important role in determining the inactivation kinetics and PIP<sub>2</sub> sensitivity of Ca<sub>v</sub>2.2 channels (Keum et al., 2014; Kim et al., 2015a, Kim et al., 2016). By manipulating the β2 constructs, we further examined how Ca<sub>v</sub> β subunits determine the gating properties of the Ca<sub>v</sub>2.2 channel depending on their subcellular localization. First, we used a palmitoylation-resistant cytosolic mutant form of β2a, β2a(C3,4S), where two palmitoylation sites (C3 and C4) in the N-terminus of the β2a subunit were mutated to serine residues (Chien et al., 1996; Hurley et al., 2000; Olcese et al., 1994; Qin et al., 1998; Figure 1A and Figure 1—figure supplement 1A). Additionally, we constructed two more membrane-recruited β2c analogs by adding membrane-targeting Lyn<sub>11</sub> (N-terminal G2-myristoylation and C3-palmitoylation modification sequence from Lyn kinase; Resh, 1994) or Lyn<sub>11</sub> plus a flexible 48 amino acid linker (Lyn-48aa) to the N-terminus of β2c. When these Ca<sub>v</sub> β constructs were expressed in cells without the pore-forming α1B, β2a(C3,4S) was distributed through the cytosol similar to β2c. By contrast, the engineered Lyn-β2c and Lyn-48aa-β2c were localized at the PM like the membrane-anchored β2a subunit (Figure 1B, C). However, in the presence of α1B and α2δ1, all the β2 constructs were mainly distributed at the PM, probably via binding to α1B subunits (Figure 1—figure supplement 1B, C). This suggested that amino acid mutation or chimeric modification of the β2 subunit does not affect the formation of the Ca<sub>v</sub>2.2 channel multicomplex. Next, we tested the effects of the β2 constructs on current inactivation and PIP<sub>2</sub> sensitivity of the Ca<sub>v</sub>2.2 channels. PIP<sub>2</sub> regulation of Ca<sub>v</sub>2.2 channel gating was measured as the difference before and after a +120 mV depolarizing pulse using Dr-VSP (see Figure 1—figure supplement 2A). Coexpression of β2a(C3,4S) accelerated current inactivation and increased the PIP<sub>2</sub> sensitivity of Ca<sub>v</sub>2.2 channels, such as those with the cytosolic β2c subunit. Expression of the chimeric Lyn-β2c slowed down the inactivation rate and decreased PIP<sub>2</sub> sensitivity, like the channels with the PM-anchored β2a subunit (Figure 1D, E). Interestingly, cells co-transfected with the PM-tethered chimeric Lyn-48aa-β2c showed faster current inactivation and higher PIP<sub>2</sub> sensitivity in Ca<sub>v</sub>2.2 channels, which were similar to the responses of channels with the cytosolic β2c subunit. In control experiments without Dr-VSP, we confirmed that the current amplitudes of Ca<sub>v</sub>2.2 channels with the developed β2 constructs were not significantly different before and after the depolarizing pulse (Figure 1—figure supplement 2A, B). Additionally, we verified that the effects of Dr-VSP were not due to relieving the Gβγ-mediated tonic inhibition from the Ca<sub>v</sub>2.2 channels. As shown in Figure 1—figure supplement 2C, prepulse depolarization did not change the current amplitudes in cells intracellularly perfused with 1 mM of the G protein inhibitor GDP-β-S instead of GTP in the absence of Dr-VSP. Moreover, the Ca<sub>v</sub>2.2 channels with GDP-β-S showed very similar PI(4,5)P<sub>2</sub> sensitivities to those in experiments with GTP in cells expressing Dr-VSP (Figure 1—figure supplement 2D). This suggested that 0.1 mM GTP concentration in the pipette solution was not sufficient to trigger spontaneous G protein activation or suppress Ca<sub>v</sub>2.2 channels through Gβγ binding.

We further examined the effects of the length of the flexible linker between Lyn and the β2c subunit on the inactivation kinetics and PIP<sub>2</sub> sensitivity of Ca<sub>v</sub>2.2 channels. As shown in Figure 1—figure supplement 3, when the inserted linkers were longer than 24 aa, current inactivation was faster and current inhibition by PIP<sub>2</sub> depletion was stronger. Together, these data suggest that the N-terminal length of the PM-tethering Ca<sub>v</sub> β subunit is critical in determining the inactivation kinetics and PIP<sub>2</sub> sensitivity of Ca<sub>v</sub>2.2 channels.

### Proximal interaction of the fatty acyl chains with channel complex underlies the β subunit-dependent regulation of Ca<sub>v</sub>2.2 channel gating

It has been previously reported that disruption of the SH3–GK interaction in the membrane-anchored β2a subunit accelerates the channel inactivation of Ca<sub>v</sub>2.1 channels (Chen et al., 2009). The GK domain of the Ca<sub>v</sub> β subunit interacts directly with the AID domain in the I–II loop of Ca<sub>v</sub> α1 subunits (Buraei and Yang, 2010; Buraei and Yang, 2013; Chen et al., 2004; Opatowsky et al., 2004; Van Petegem et al., 2004); therefore, disruption of the SH3–GK interaction in the Ca<sub>v</sub> β subunit may increase the length between the N-terminus and the GK–AID complex through the flexible HOOK region. To test the possible effects of increased N-terminal length from the AID–GK complex on Ca<sub>v</sub>

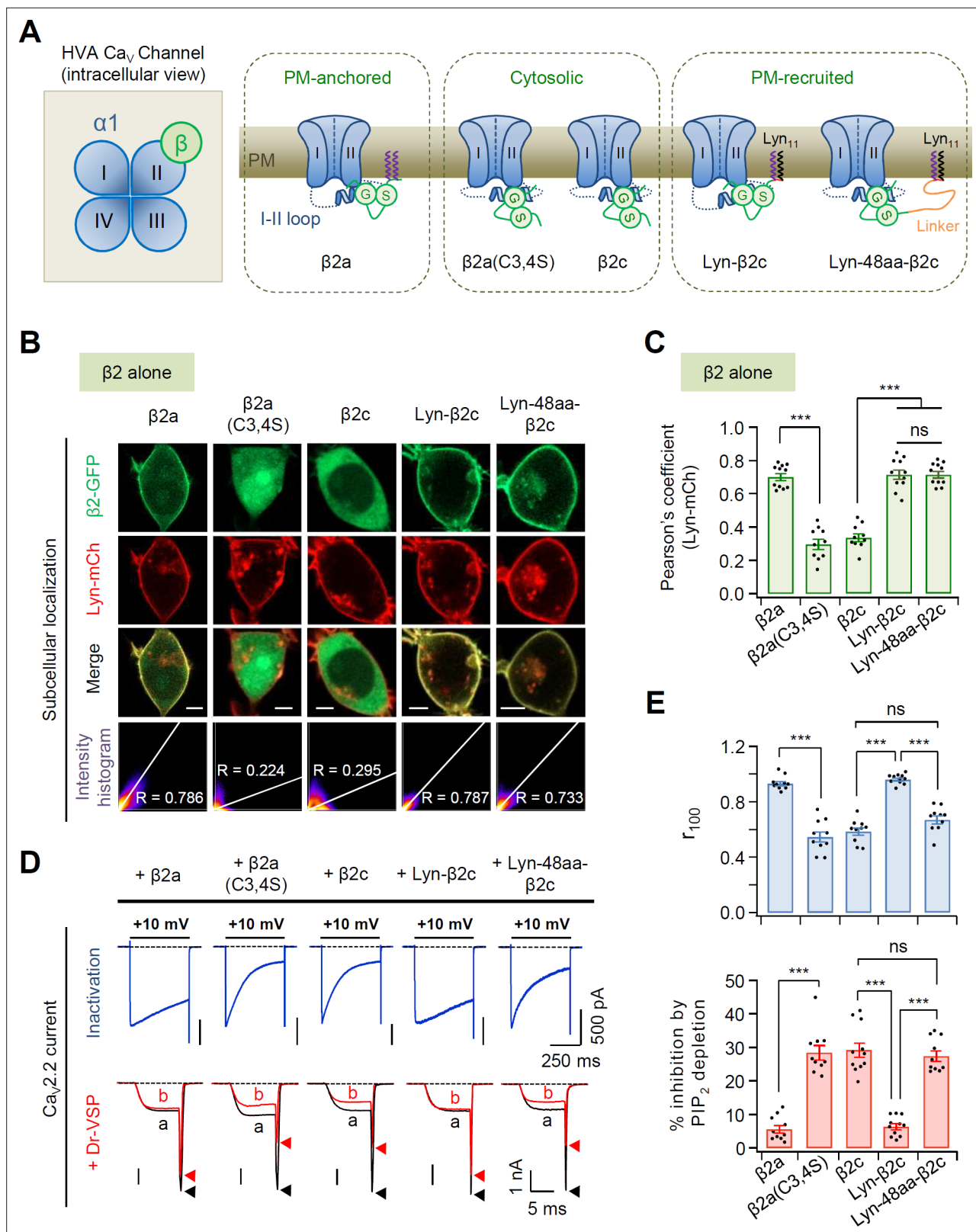


**Figure 1.** Current inactivation and PIP<sub>2</sub> sensitivity in N-type Ca<sub>v</sub>.2.2 channels with different subtypes of the  $\beta 2$  subunit. **(A)** Schematic diagram of high-voltage-activated (HVA) calcium channel complex viewed from the intracellular side (left). Ca<sub>v</sub>  $\beta$  subunit is located beside the domain II of  $\alpha 1B$  in the cytosolic side while Ca<sub>v</sub>  $\alpha 2\delta$  subunit is mostly localized at the extracellular surface of the channel protein (Gao et al., 2021). Schematic model of Ca<sub>v</sub>.2.2 channels with plasma membrane (PM)-anchored  $\beta 2a$ , cytosolic  $\beta 2a(C3,4S)$  and  $\beta 2c$ , or N-terminus engineered PM-recruited  $\beta 2c$  (right). **(B)**

Figure 1 continued on next page

## Figure 1 continued

Representative confocal images of tsA-201 cells expressing the PM marker Lyn-mCh and  $\beta 2$  isoforms or its derivatives fused to GFP without the  $\alpha 1$  and  $\alpha 2\delta 1$  subunits. Scale bar, 5  $\mu\text{m}$ . The scatter plot shows a 2D intensity histogram of the red (Lyn-mCh) and green ( $\beta 2$ -GFP) pixels in the confocal image. The value indicates the Pearson's correlation coefficient ( $R$ ) that is obtained by the Colocalization Threshold plugin of Fiji software (Image J). (C) Summary of Pearson's coefficient between Lyn-mCh and the  $\beta 2$  construct ( $n = 10-11$ ). (D) Current inactivation of  $\text{Ca}_v 2.2$  channels with  $\beta 2$  isoforms or its derivatives was measured during 500-ms test pulses to +10 mV (top). Current inhibition of  $\text{Ca}_v 2.2$  channels by Dr-VSP-mediated  $\text{PIP}_2$  depletion (bottom). The current traces before (a) and after (b) the strong depolarizing pulse to +120 mV were superimposed. Peak tail current is indicated by arrowheads (trace a, black head; trace b, red head). (E) Summary of current inactivation (top;  $n = 10-11$ ) and inhibition (%) by  $\text{PIP}_2$  depletion (bottom;  $n = 10-11$ ) in  $\text{Ca}_v 2.2$  channels with the  $\beta 2$  constructs.  $r_{100}$  indicates the fraction of current remaining after 100-ms depolarization to +10 mV (top). Dots indicate the individual data points for each cell. Data are mean  $\pm$  standard error of the mean (SEM). \*\*\* $p < 0.001$ , using one-way analysis of variance (ANOVA) followed by Tukey post hoc test.

The online version of this article includes the following source data and figure supplement(s) for figure 1:

**Source data 1.** Current inactivation ( $r_{100}$ ) and current inhibition (%) by  $\text{PIP}_2$  depletion in N-type  $\text{Ca}_v 2.2$  channels with different subtypes of the  $\beta 2$  subunit.

**Figure supplement 1.** Subcellular localization of N-terminus engineered constructs of  $\beta 2$  subunit in the presence of  $\alpha 1$  and  $\alpha 2\delta 1$  subunits.

**Figure supplement 1—source data 1.** Pearson's coefficient between Lyn-mCh and the  $\beta 2$  construct in the presence of  $\alpha 1$  and  $\alpha 2\delta 1$  subunit.

**Figure supplement 2.** Summary of the  $\text{Ca}_v 2.2$  current inhibition by a 120-mV-depolarizing pulse in cells without or with Dr-VSP.

**Figure supplement 2—source data 1.** Current inhibition (%) by a depolarizing pulse in cells in the absence of Dr-VSP.

**Figure supplement 2—source data 2.** Summary of the  $\text{Ca}_v 2.2$  current inhibition by Dr-VSP-mediated  $\text{PIP}_2$  depletion in cells were recorded with pipette solution containing GDP- $\beta$ -S.

**Figure supplement 3.** Effects of inserting a flexible linker between Lyn and  $\beta 2c$  subunit on current inactivation and  $\text{PIP}_2$  sensitivity of  $\text{Ca}_v 2.2$  channels.

**Figure supplement 3—source data 1.** Current inactivation ( $r_{100}$ ) and current inhibition (%) by  $\text{PIP}_2$  depletion in  $\text{Ca}_v 2.2$  channels with chimeric Lyn-linker- $\beta 2c$  derivatives.

channel gating, we constructed mutant  $\beta 2a$  subunits in which the SH3-GK intramolecular interaction was disrupted by mutating seven amino acids in the SH3 and GK domains to alanine residues (**Figure 2A**). Additionally, the N-terminus was deleted to abolish membrane targeting of the  $\beta 2a$  subunit by itself, and Lyn<sub>11</sub> was inserted to the N-terminus for membrane recruitment. Without  $\alpha 1B$  and  $\alpha 2\delta 1$ , both N-terminus-deleted ( $\Delta\text{N}$ ) $\beta 2$  WT and ( $\Delta\text{N}$ ) $\beta 2$  Mut, in which the SH3-GK interaction was disrupted, were expressed in the cytosol. Conversely, Lyn-( $\Delta\text{N}$ ) $\beta 2$  WT and Lyn-( $\Delta\text{N}$ ) $\beta 2$  Mut constructs were localized to the PM (**Figure 2A**, inset images). In  $\text{Ca}_v 2.2$  channels with the N-terminus-deleted mutant ( $\Delta\text{N}$ ) $\beta 2$  WT, the current exhibited fast inactivation and high  $\text{PIP}_2$  sensitivity (**Figure 2B-D**). These phenomena similarly appeared in channels with the ( $\Delta\text{N}$ ) $\beta 2$  Mut. In contrast,  $\text{Ca}_v 2.2$  channels with Lyn-( $\Delta\text{N}$ ) $\beta 2$  WT exhibited slow inactivation and weak  $\text{PIP}_2$  sensitivity. However, the channels with Lyn-( $\Delta\text{N}$ ) $\beta 2$  Mut exhibited fast inactivation and strong  $\text{PIP}_2$  sensitivity, like channels with cytosolic ( $\Delta\text{N}$ ) $\beta 2$  WT and ( $\Delta\text{N}$ ) $\beta 2$  Mut (**Figure 2B-D**). We also confirmed that disruption of the SH3-GK interaction did not shift the current-voltage ( $I$ - $V$ ) curve of  $\text{Ca}_v 2.2$  currents (**Figure 2—figure supplement 1**). These data suggested that the length from the N-terminal lipid anchor to the GK domain of  $\beta$  subunit is crucial in determining the inactivation rate and  $\text{PIP}_2$  sensitivity of  $\text{Ca}_v 2.2$  channels.

To further examine the functional role of length between lipid anchor and GK domain on  $\text{Ca}_v$  channel gating in live cells, we developed new chimeric  $\beta 2$  constructs by applying the rapamycin-induced dimerizing system FK506-binding protein (FKBP) and FKBP-rapamycin-binding (FRB) protein (**Banaszynski et al., 2005; Inoue et al., 2005; Suh et al., 2006**). As shown in **Figure 3A**, FKBP and FRB proteins irreversibly assembled to form a ternary complex upon application of rapamycin, which led to shortening of the length between the lipid anchor Lyn<sub>11</sub> and GK-AID domains. We fused a Förster resonance energy transfer (FRET) probe YFP to the C-terminus of all  $\beta 2$  chimera to investigate whether the FKBP domain was really translocated to the PM to make a Lyn<sub>11</sub>-FRB and FKBP complex closely after rapamycin addition (**Figure 3A**, right diagram). In experiments with the  $\beta$  chimera without the FKBP domain (Control: Lyn-FRB-HOOK-GK), both FRET<sub>r</sub> and the current amplitude of  $\text{Ca}_v 2.2$  channels were not changed by rapamycin addition (**Figure 3B**). Consistently, rapamycin treatment did not affect current inactivation and the  $\text{PIP}_2$  sensitivity of  $\text{Ca}_v 2.2$  channels in these cells (**Figure 3C-F**). In contrast, in  $\text{Ca}_v 2.2$  channels with Lyn-FRB-HOOK-GK-FKBP (RF), rapamycin treatment irreversibly enhanced the FRET<sub>r</sub> signal and increased the current amplitude of  $\text{Ca}_v 2.2$  channels (**Figure 3B**, middle and **Figure 3—figure supplement 1**). Moreover, rapamycin treatment reduced the current inactivation and  $\text{PIP}_2$  sensitivity of  $\text{Ca}_v 2.2$  channels (**Figure 3C-F**). However, in  $\text{Ca}_v 2.2$  channels with

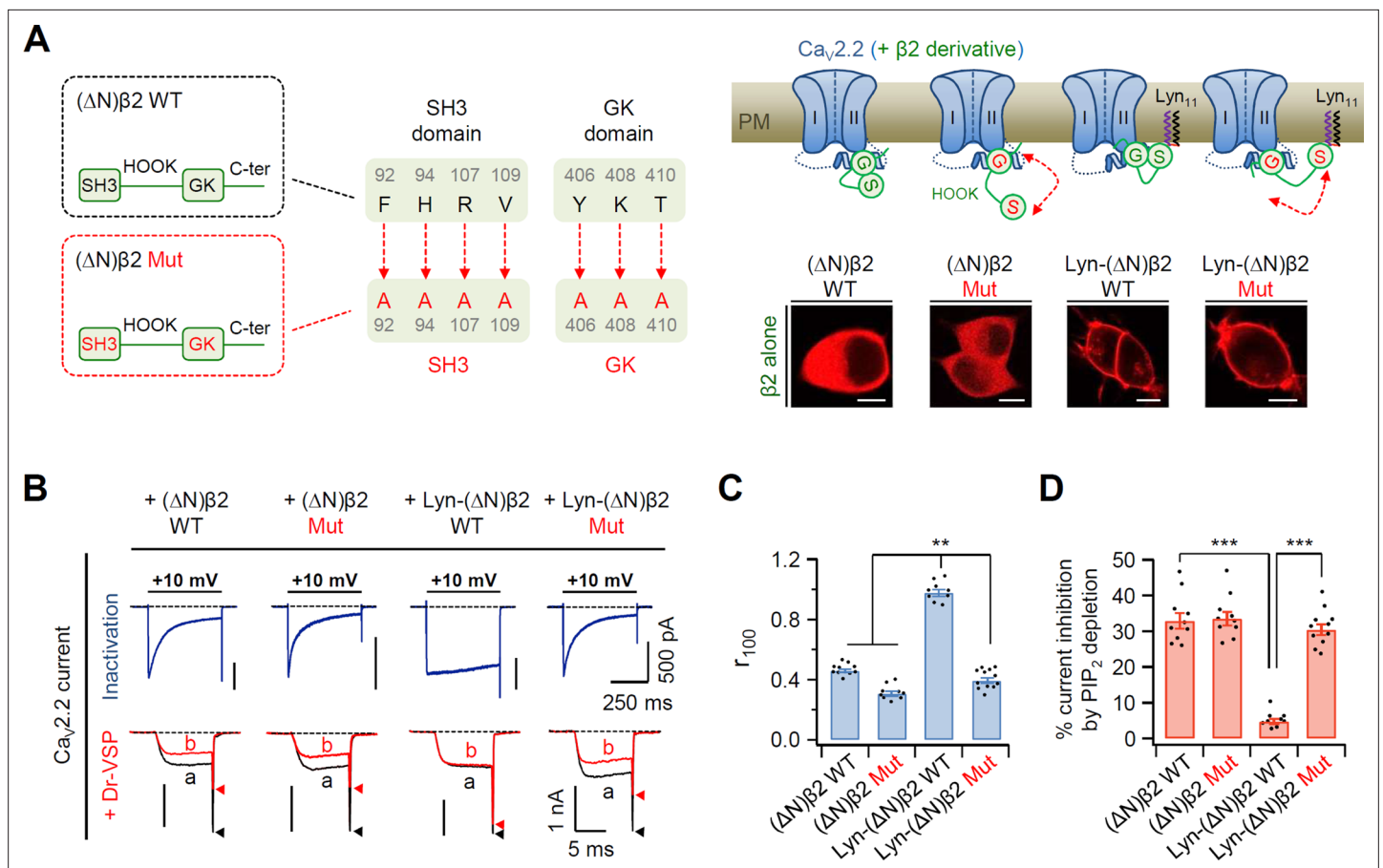


**Figure 2.** Disruption of SH3–GK interaction in the plasma membrane (PM)-recruited  $Ca_v2.2$  channels leads to an increase in both current inactivation and PIP<sub>2</sub> sensitivity of  $Ca_v2.2$  channels. **(A)** Left, a diagram showing how the SH3–GK intramolecular interaction is disrupted in  $\beta_2$  constructs (top). Phenylalanine 92, histidine 94, arginine 107, and valine 109 residues in the SH3 domain and tyrosine 406, lysine 408, and threonine 410 residues in the GK domain are replaced with alanine. Schematic model of  $Ca_v2.2$  channels with engineered  $\beta_2$  constructs in which the SH3–GK intramolecular interaction is disrupted. Lyn-( $\Delta$ N) $\beta_2$ : Lyn-labeled N-terminus-deleted  $\beta_2$  construct. Lyn-( $\Delta$ N) $\beta_2$  Mut: Lyn-( $\Delta$ N) $\beta_2$  construct with a disrupted SH3–GK intramolecular interaction. Inset: confocal images of tsA-201 cells expressing engineered  $\beta_2$  constructs labeled with mCherry without  $\alpha_1B$  and  $\alpha_2\delta_1$  subunits. Scale bar, 5  $\mu$ m. **(B)** Representative currents of  $Ca_v2.2$  channels with engineered  $\beta_2$  constructs. The currents were measured during 500-ms test pulses to +10 mV (top). Current traces before (a) and after (b) a +120-mV depolarizing pulse in cells expressing  $Ca_v2.2$  channels with engineered  $\beta_2$  constructs and Dr-VSP (bottom). Peak tail current is indicated by arrowheads (trace a, black head; trace b, red head). **(C)** Summary of  $Ca_v2.2$  current inactivation ( $n = 9$ –12).  $r_{100}$  indicates the fraction of current remaining after 100-ms depolarization to +10 mV. **(D)** Summary of  $Ca_v2.2$  current inhibitions (%) by PIP<sub>2</sub> depletion in Dr-VSP-expressing cells ( $n = 9$ –11). Dots indicate the individual data points for each cell. Data are mean  $\pm$  standard error of the mean (SEM). \*\* $p < 0.01$ , \*\*\* $p < 0.001$ , using one-way analysis of variance (ANOVA) followed by Tukey post hoc test.

The online version of this article includes the following source data and figure supplement(s) for figure 2:

**Source data 1.** Current inactivation ( $r_{100}$ ) and current inhibition (%) by PIP<sub>2</sub> depletion in N-type  $Ca_v2.2$  channels with the engineered  $\beta_2$  construct.

**Figure supplement 1.** Disruption of the SH3–GK intramolecular interaction of  $\beta_2$  subunit does not shift current–voltage ( $I$ – $V$ ) curve of  $Ca_v2.2$  current.

**Figure supplement 1—source data 1.** Current–voltage ( $I$ – $V$ ) curve of  $Ca_v2.2$  current.

Lyn-FRB-HOOK-GK-Linker-FKBP (RCF), where a 194-aa linker was inserted between GK and FKBP, rapamycin enhanced the FRET signal without causing significant changes in the current amplitude (Figure 3B, right and Figure 3—figure supplement 1). The effects of rapamycin on inactivation kinetics and PIP<sub>2</sub> sensitivity were much weaker in  $Ca_v2.2$  channels with RCF when compared with those in channels with RF (Figure 3C–F). This suggested that rapamycin-induced dimerization may be insufficient to shorten the length between the lipid anchor and isolated GK domain of  $\beta$  subunit in channels with RCF.

Next, we measured the effects of the N-terminal length of PM-tethered  $\beta$  subunit on  $Ca_v2.2$  channel activity by inserting flexible linkers of various lengths between Lyn<sub>11</sub> and the GK domain of  $\beta_2$

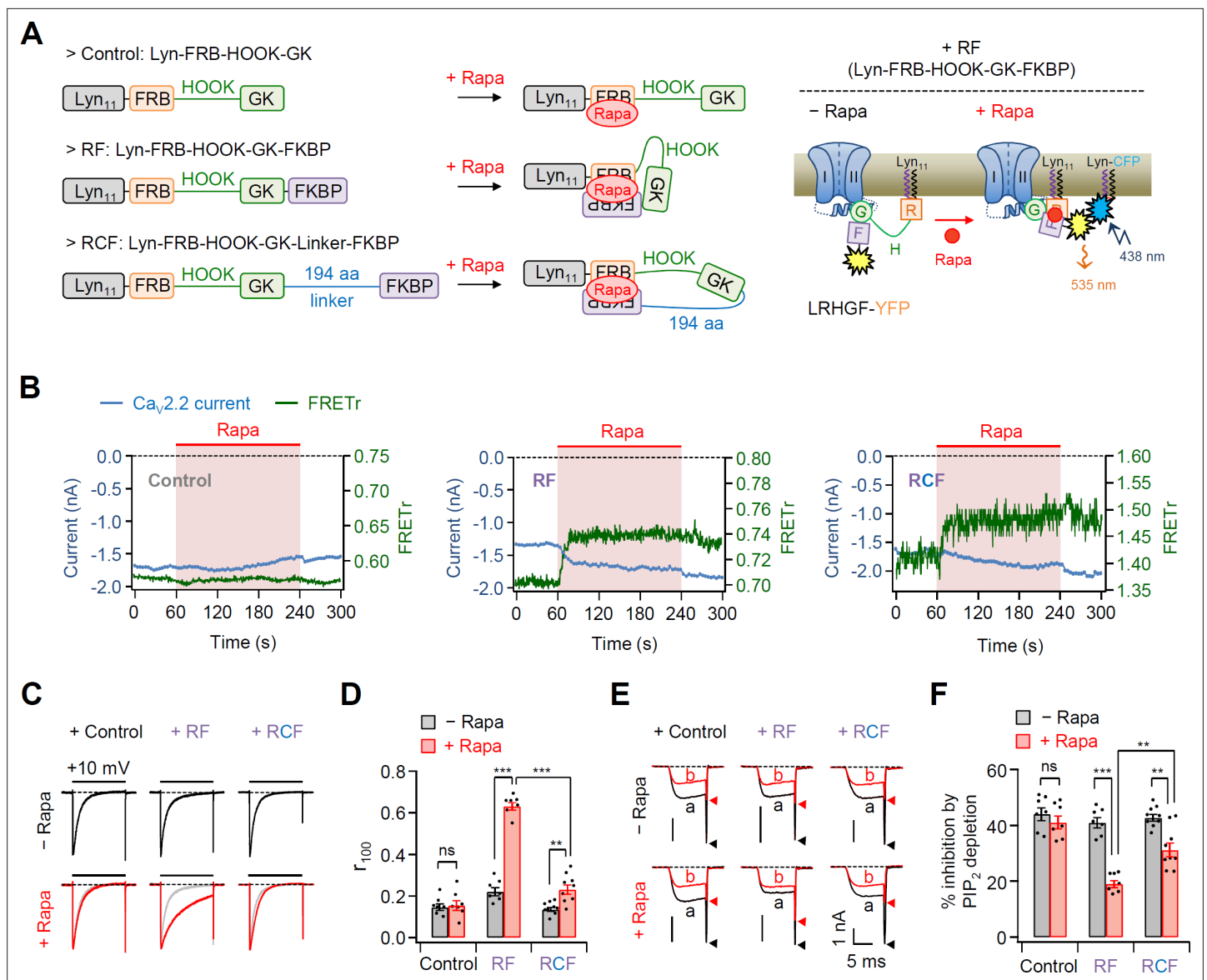


**Figure 3.** Effects of the real-time translocation of the GK domain to the plasma membrane (PM) on  $Ca_v2.2$  channel gating. **(A)** Left, a schematic diagram showing rapamycin-induced translocatable  $\beta 2$  chimeric constructs. Translocatable  $\beta 2$  chimeric constructs were invented by fusing FRB or FKBP to the N- and C-termini of the GK domain, respectively. The new constructs were tagged with  $Lyn_{11}$  (RF or Lyn-FRB-Hook-GK-FKBP) to be tethered to the PM. Rapamycin (Rapa) addition triggers the formation of a tripartite FRB–rapamycin–FKBP complex, resulting in the movement of the FKBP domain to the PM (right). For Förster resonance energy transfer (FRET) imaging, chimeric  $\beta$  constructs labeled with YFP in the C-terminus and PM-targeting Lyn-CFP were coexpressed. Right, schematic model of  $Ca_v2.2$  channels with RF before and after rapamycin application. Rapamycin induces the formation of the tripartite complex, resulting in a shift of the FKBP domain to the PM and an enhanced FRET signal. **(B)** Time courses of  $Ca_v2.2$  currents (blue traces) and FRET ratio (green traces) were measured simultaneously in single cells expressing  $Ca_v2.2$  channels with Cont (left), RF (middle), or RCF (right) and the membrane marker Lyn-CFP. **(C)** Current inactivation of  $Ca_v2.2$  channels with Cont (left), RF (middle), and RCF (right) was measured during 500-ms test pulses to +10 mV before (black traces) and after (red traces) rapamycin addition. **(D)** Summary of inactivation of  $Ca_v2.2$  currents before (black bars) and after (red bars) rapamycin application ( $n = 7-9$ ). The fraction of the current remaining after 100-ms depolarization ( $r_{100}$ ) to +10 mV. **(E)** Current inhibition of Dr-VSP-mediated  $PIP_2$  depletion on  $Ca_v2.2$  channels with Cont (left), RF (middle), and RCF (right) before and after rapamycin addition. The traces before **(a)** and after **(b)** the depolarizing pulse to +120 mV were superimposed. Peak tail current is indicated by arrowheads (trace a, black head; trace b, red head). **(F)** Summary of Dr-VSP-induced  $Ca_v2.2$  current inhibition before (black bars) and after (red bars) rapamycin addition ( $n = 7-9$ ). Dots indicate the individual data points for each cell. Data are mean  $\pm$  standard error of the mean (SEM). \*\* $p < 0.01$ , \*\*\* $p < 0.001$ , using two-way analysis of variance (ANOVA) followed by Sidak post hoc test.

The online version of this article includes the following source data and figure supplement(s) for figure 3:

**Source data 1.** Time courses of  $Ca_v2.2$  currents and Förster resonance energy transfer (FRET) ratio.

Figure 3 continued on next page

Figure 3 continued

**Source data 2.** Current inactivation ( $r_{100}$ ) and current inhibition (%) by  $\text{PIP}_2$  depletion in  $\text{Ca}_v2.2$  channels with rapamycin-induced translocatable  $\beta 2$  chimeric constructs before and after rapamycin.

**Figure supplement 1.** The real-time translocation of the GK domain to the plasma membrane increased the current amplitude of  $\text{Ca}_v2.2$  channels.

**Figure supplement 1—source data 1.** Relative peak current amplitudes of  $\text{Ca}_v2.2$  channels with chimeric Lyn-linker- $\beta 2c$  derivatives.

(Figure 4A). The inserted linkers were unstructured flexible peptides (see Figure 4—figure supplement 1); therefore, the length of the linkers was calculated using the worm-like chain (WLC) model (see Methods). Our results showed that both the current inactivation and  $\text{PIP}_2$  sensitivity of  $\text{Ca}_v2.2$  channels became gradually stronger as the inserted flexible linkers became longer (Figure 4B–D). Consistently, the current activation was gradually accelerated by the increase in linker length (Figure 4—figure supplement 2). However, no additional difference was detected in channels with the membrane-tethered Lyn-43aa-GK subunit when compared with the cytosolic GK subunit. This indicated that the GK domain with the length of the inserted 43-aa linker is sufficient to act like the cytosolic  $\text{Ca}_v \beta$  subunit (Figure 4B–D). Interestingly, the  $\text{PIP}_2$  sensitivity and inactivation kinetics of  $\text{Ca}_v$  channels were differentially regulated by the length between the lipid anchor and the GK domain: the channels with Lyn-43aa-GK showed faster inactivation than the channels with Lyn-22aa-GK, whereas the  $\text{PIP}_2$  sensitivity of the two channels was not significantly different (Figure 4B–E). Additionally, our data analysis indicated that the biophysical gating properties of  $\text{Ca}_v2.2$  channels with a membrane-anchored  $\beta 2a$  subunit were similar to those of channels with Lyn-9aa-GK. Furthermore, the gating properties of  $\text{Ca}_v2.2$  channels coupled with cytosolic  $\beta 2c$  were similar to those of channels with Lyn-20aa-GK (Figure 4E).

Previous studies have reported that subcellular localization of the  $\text{Ca}_v \beta$  subunit is important in determining the current density of  $\text{Ca}_v$  channels, where  $\text{Ca}_v$  channels with the membrane-anchored  $\beta$  subunit show relatively higher current density than channels with the cytosolic  $\beta$  subunit (Suh et al., 2012). In line with this, we found that the current density of  $\text{Ca}_v2.2$  channels with  $\beta 2a$  was significantly higher than that of channels with  $\beta 2c$  (Figure 4—figure supplement 3A–C). Therefore, we tested whether the current density of  $\text{Ca}_v$  channels was dependent on the N-terminal length.  $\text{Ca}_v2.2$  channels showed slightly decreased current density that was dependent on the expansion of the flexible linker length between Lyn and the GK domain alone (Figure 4—figure supplement 4A, C). This phenomenon was observed in channels with the whole  $\beta 2c$  subunit with Lyn (Figure 4—figure supplement 3D–F). We tested whether the length between N-terminal lipid anchor and GK domain affected the voltage-dependent gating of  $\text{Ca}_v$  channels. Voltage-dependent activation of  $\text{Ca}_v2.2$  channels with Lyn-linker-GK derivatives showed a greater shift to positive voltage as the inserted flexible linkers increased in length (Figure 4—figure supplement 4B, D). This suggested that incremental increases in linker length lead to a decreased voltage sensitivity. There was no difference in the current density and voltage-dependent activation between  $\text{Ca}_v$  channels with the Lyn-43aa-GK and GK subunit. Together, these results suggested that differential regulation of  $\text{Ca}_v2.2$  channel gating by  $\beta$  subunits is mainly determined by the anchoring properties of the  $\beta$  subunits to PM.

## Polybasic motif at the C-terminal end of I-II loop plays an important role in the $\text{PIP}_2$ regulation of $\text{Ca}_v2.2$ channels

How does the N-terminal length of the PM-tethering  $\text{Ca}_v \beta$  subunit regulate  $\text{Ca}_v$  channel gating? Recently, Kaur et al., 2015 have reported that a polybasic motif consisting of four basic amino acids within the C-terminal end of the I-II loop of L-type  $\text{Ca}_v1.2$  channels interacts with membrane phospholipids, including  $\text{PIP}_2$ . Additionally, the putative  $\text{PIP}_2$ -binding site is conserved in the I-II loop of N-type  $\text{Ca}_v2.2$  channels (Figure 5—figure supplement 1). We examined whether the polybasic motif affects the  $\text{PIP}_2$  sensitivity of  $\text{Ca}_v2.2$  channels. First, we eliminated the potential phospholipid-binding motif from the  $\text{Ca}_v2.2$  channel I-II loop by mutating the four polybasic residues to alanine (4A  $\alpha 1B$ ) (Figure 5A). In  $\text{Ca}_v2.2$  channels with the  $\beta 2a$  subunit, the inactivation kinetics of the current did not differ between WT  $\alpha 1B$  and 4A  $\alpha 1B$  (Figure 5B, C, left). However, in  $\text{Ca}_v2.2$  with  $\beta 2c$ , the inactivation rate was slower in 4A  $\alpha 1B$  channels (Figure 5B, C, right). The effects of  $\text{PIP}_2$  depletion on current amplitude were also measured in these channels. In control experiments without Dr-VSP, the current of WT or 4A-mutant  $\text{Ca}_v2.2$  channels did not significantly differ before and after a +120-mV depolarizing



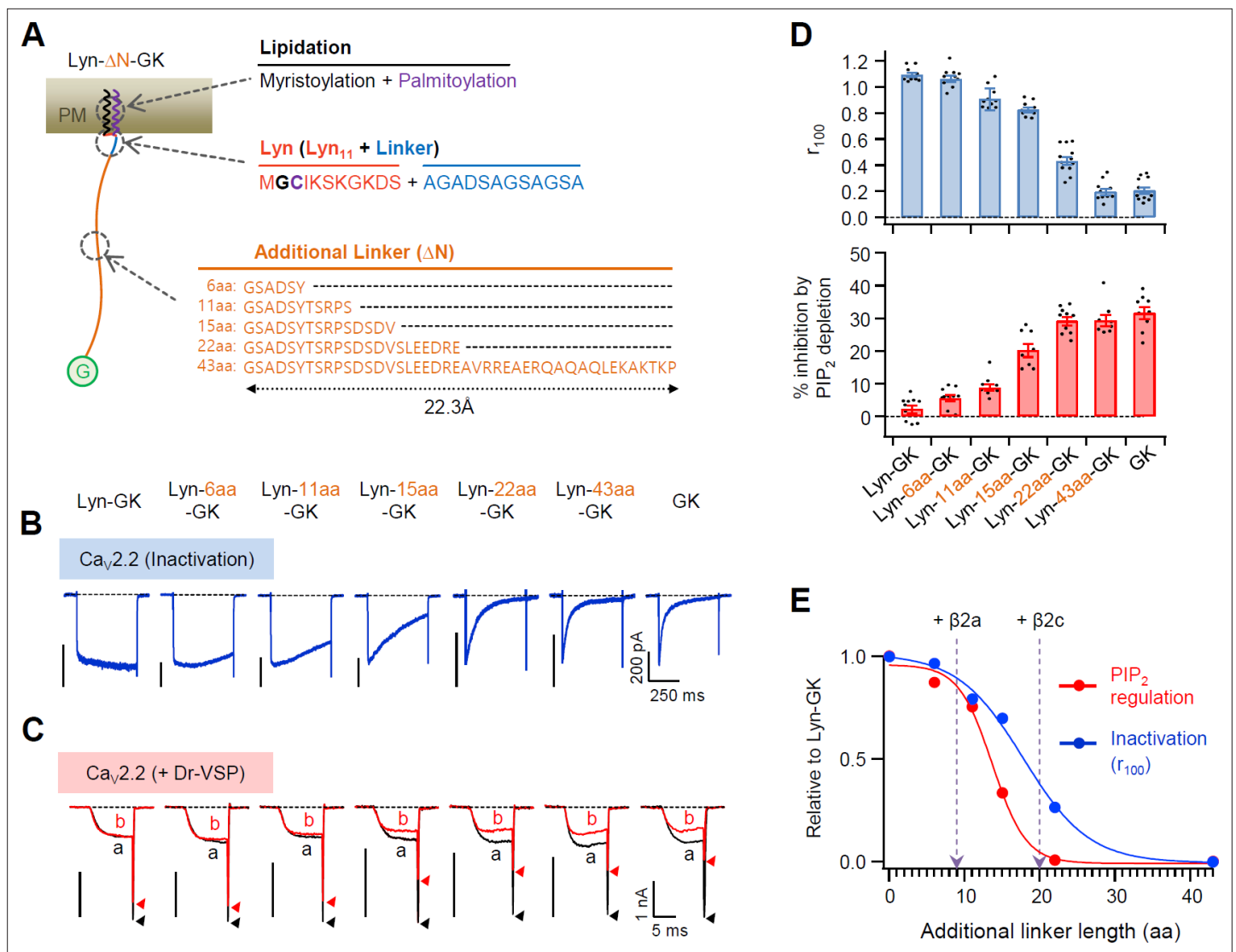


**Figure 4.** Flexible linker length between Lyn and the GK domain of the  $\beta$  subunit performs a key role in determining both the current inactivation and the PIP<sub>2</sub> sensitivity of Ca<sub>v</sub>2.2 channels. **(A)** Schematic diagram of diverse flexible linkers ( $\Delta$ N) inserted between Lyn and GK (G) domain. The length of each linker is calculated by the worm-like chain (WLC) model (see Methods). Amino acid sequences of Lyn (Lyn<sub>11</sub> plus 12 aa linker) and the additional linkers are listed. **(B)** Current inactivation of Ca<sub>v</sub>2.2 channels with diverse Ca<sub>v</sub>  $\beta$ -GK derivatives was measured during 500 ms test pulses to +10 mV. **(C)** Effects of Dr-VSP-mediated PIP<sub>2</sub> depletion on Ca<sub>v</sub>2.2 channels with GK domain derivatives. Peak tail current is indicated by arrowheads (trace a, black head; trace b, red head). **(D)** Summary of current inactivation (blue bars;  $n = 9-12$ ) and inhibition (%) by PIP<sub>2</sub> depletion (red bars;  $n = 8-10$ ) in Ca<sub>v</sub>2.2 channels with Ca<sub>v</sub>  $\beta$  GK derivatives. Data are mean  $\pm$  standard error of the mean (SEM). Dots indicate the individual data points for each cell. **(E)** Normalized mean current inactivation and mean current inhibition by PIP<sub>2</sub> depletion versus additional linker length (aa) of Ca<sub>v</sub>  $\beta$  GK derivatives measured in Ca<sub>v</sub>2.2 channels. The normalized current regulation in cells expressing Ca<sub>v</sub>2.2 with  $\beta$ 2a and  $\beta$ 2c is indicated with dashed arrows.

The online version of this article includes the following source data and figure supplement(s) for figure 4:

**Source data 1.** Current inactivation ( $r_{100}$ ) and current inhibition (%) by PIP<sub>2</sub> depletion in Ca<sub>v</sub>2.2 channels with the engineered  $\beta$ 2 GK derivatives.

**Figure supplement 1.** IUPRED web-server result of inserted linker.

**Figure supplement 2.** Summary of time constants for Ca<sub>v</sub>2.2 current activation.

**Figure supplement 2—source data 1.** Time constants of current activation in Ca<sub>v</sub>2.2 channels with diverse Ca<sub>v</sub>  $\beta$ -GK derivatives.

**Figure supplement 3.** Current density in N-type Ca<sub>v</sub>2.2 channels with  $\beta$ 2 variants.

**Figure supplement 3—source data 1.** Population current density versus voltage relations for Ca<sub>v</sub>2.2 channels with  $\beta$ 2 variants.

**Figure supplement 4.** Flexible linker length between Lyn and GK domain of  $\beta$  subunit is important in determining the current density and the voltage-dependent gating of Ca<sub>v</sub>2.2 channels.

Figure 4 continued on next page

Figure 4 continued

**Figure supplement 4—source data 1.** Population current density versus voltage relations and the voltage dependence of normalized steady-state activation for  $\text{Ca}_v2.2$  channels with the engineered  $\beta 2$  GK derivatives.

pulse in cells with either  $\beta 2a$  or  $\beta 2c$  subunits (**Figure 5D**). By contrast,  $\text{PIP}_2$  depletion by Dr-VSP activation similarly inhibited the  $\text{Ca}_v$  current by approximately 5% in cells expressing either WT or 4A  $\text{Ca}_v2.2$  channels with a PM-anchored  $\beta 2a$  subunit (**Figure 5E**, left). This indicated the presence of another  $\text{PIP}_2$ -binding site in the  $\alpha 1B$  subunit other than this polybasic motif in I-II loop. On the other hand, the  $\text{PIP}_2$  sensitivity in channels with  $\beta 2c$  was dramatically reduced in 4A channels, indicating that the polybasic motif in the I-II loop plays a key role in  $\text{PIP}_2$  regulation of  $\text{Ca}_v2.2$  channels with the cytosolic  $\beta$  subunit (**Figure 5D, E**). However, in cells expressing 4A  $\text{Ca}_v2.2$  channels with  $\beta 2c$ , we observed another ~5% current inhibition by  $\text{PIP}_2$  depletion. This was similar to the  $\text{Ca}_v2.2$  channels with  $\beta 2a$ .

Next, we investigated whether the polybasic motif affects the  $\text{PIP}_2$  sensitivity of  $\text{Ca}_v2.2$  channels with Lyn- $\beta 2c$  and Lyn-48aa- $\beta 2c$  (**Figure 5—figure supplement 2**). Similar to  $\beta 2a$ , we did not detect any significant differences in current inactivation and  $\text{PIP}_2$  sensitivity between WT and 4A mutant  $\text{Ca}_v2.2$  with Lyn- $\beta 2c$  (**Figure 5—figure supplement 2**). Conversely, WT  $\text{Ca}_v2.2$  channels with Lyn-48aa- $\beta 2c$  exhibited faster inactivation and higher  $\text{PIP}_2$  sensitivity, which was similar to the responses of  $\text{Ca}_v2.2$  channels with cytosolic  $\beta 2c$ . However, in cells expressing 4A mutant  $\text{Ca}_v2.2$  channels with Lyn-48aa- $\beta 2c$ , the current inactivation was slowed and the  $\text{PIP}_2$  sensitivity was decreased to ~5% (**Figure 5—figure supplement 2**). The  $\text{PIP}_2$  sensitivities of 4A  $\text{Ca}_v2.2$  channels with Lyn- $\beta 2c$  and Lyn-48aa- $\beta 2c$  did not significantly differ and were similar to that of WT channels with Lyn- $\beta 2c$ . Consistent with the data in **Figure 5**, these results suggested that the polybasic motif within the I-II loop interacts with membrane  $\text{PIP}_2$  in  $\text{Ca}_v2.2$  channels with  $\beta 2c$ -like Lyn-48aa- $\beta 2c$ , but not with  $\beta 2a$ -like Lyn- $\beta 2c$  subunits. On the other hand, in channels with the  $\beta 2a$  subunit, there was no significant difference in the voltage-dependent activation between WT  $\alpha 1B$  and 4A  $\alpha 1B$  (**Figure 5F, G**). However, the activation of 4A  $\alpha 1B$  with the  $\beta 2c$  subunit was significantly shifted toward the hyperpolarization direction when compared with WT  $\alpha 1B$  channels with  $\beta 2c$  (**Figure 5F, G**). In addition, the activation curve of 4A  $\alpha 1B$  with  $\beta 2c$  was similar to the curves of WT and 4A  $\alpha 1B$  with  $\beta 2a$  (**Figure 5F, G**). Together, our data suggested that two different  $\text{PIP}_2$ -interacting sites with differential  $\text{PIP}_2$  sensitivities exist in  $\text{Ca}_v2.2$  channels. More importantly, our data indicate that  $\text{PIP}_2$  interacts with the polybasic motif when  $\text{Ca}_v2.2$  is expressed with cytosolic  $\beta$  subunits but not when expressed with lipidated membrane-anchored  $\beta$  subunit.

Finally, we determined whether other arginine residues in the distal region of polybasic motif also affected the  $\text{PIP}_2$  sensitivity of  $\text{Ca}_v2.2$  channels (**Figure 5—figure supplement 3**). For this, two arginine residues (R476 and R477) near the polybasic motif were replaced with alanine ( $\alpha 1B$  R476,477A) (**Figure 5—figure supplement 3A**). We also constructed a  $\alpha 1B$  R465,466A by mutating only two arginine residues (R465 and R466) in the polybasic motif (R465, R466, K469, and R472) (**Figure 5—figure supplement 3A**). In  $\text{Ca}_v2.2$  channels with the  $\beta 2a$  subunit, we did not detect any significant differences in current inactivation and  $\text{PIP}_2$  sensitivity among WT  $\alpha 1B$ ,  $\alpha 1B$  R465,466A, and  $\alpha 1B$  R476,477A (**Figure 5—figure supplement 3B–E**). However, in  $\text{Ca}_v2.2$  with  $\beta 2c$ , the inactivation rate was slower and the  $\text{PIP}_2$  sensitivity was weaker in both  $\alpha 1B$  R465,466A and  $\alpha 1B$  R476,477A compared to WT  $\alpha 1B$  (**Figure 5—figure supplement 3B–E**).

### Differential modulation of $\text{Ca}_v2.2$ channels by muscarinic receptor stimulation in cells expressing PM-anchored or cytosolic $\beta$ subunit

To examine whether the polybasic motif influenced the  $G_q$ -coupled modulation of  $\text{Ca}_v2.2$  channels, we applied the muscarinic acetylcholine receptor agonist, oxotremorine-M (Oxo-M), to cells co-transfected with the  $M_1$  muscarinic receptor ( $M_1R$ ) (**Figure 6**). Since the  $M_1R$  stimulation suppressed  $\text{Ca}_v2.2$  channels through both  $G\beta\gamma$  binding to channels and  $\text{PIP}_2$  depletion (*Keum et al., 2014*), we then used a  $G\beta\gamma$ -insensitive chimeric  $\text{Ca}_v2.2$  channel construct,  $\alpha 1C$ -1B, to examine the effect of  $\text{PIP}_2$  depletion alone on channel regulation (**Figure 6**). In this chimera construct, the N-terminus of  $\text{Ca}_v2.2$  ( $\alpha 1B$ ), which contains one of the  $G\beta\gamma$  interaction sites, is replaced by the N-terminus of  $\text{Ca}_v1.2$  ( $\alpha 1C$ ) (*Agler et al., 2005*).  $M_1R$  activation inhibited the current by approximately 5% in cells expressing either  $\alpha 1C$ -1B WT or 4A channels with  $\beta 2a$  subunit, which were similar to the responses of regulation by Dr-VSP-mediated  $\text{PIP}_2$  depletion in those channels (**Figure 6B, C**). However, consistent with the results

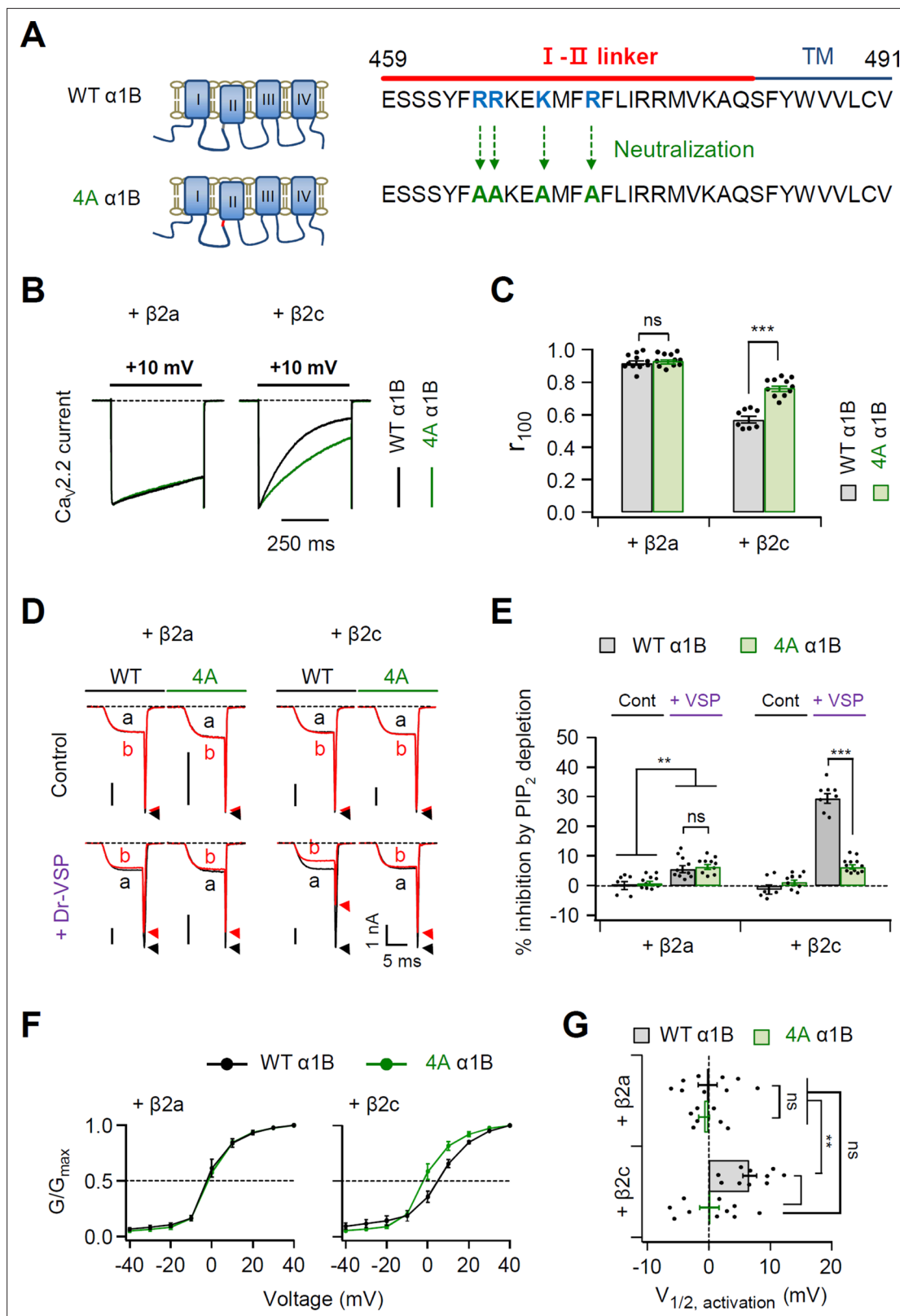


**Figure 5.** Polybasic motif at the C-terminal end of the I-II loop influences determination of steady-state activation, current inactivation, and  $PIP_2$  sensitivity of  $Ca_v2.2$  channels. **(A)** Schematic diagram of phospholipid-binding residue-neutralizing mutations within the C-terminal end of the I-II loop in the  $\alpha 1B$  subunit. The phospholipid-binding residues (R465, R466, K469, and R472) highlighted in blue were mutated to alanine (4A). **(B)** Current inactivation was measured during 500-ms test pulses to +10 mV in cells expressing  $\alpha 1B$  WT (black traces) and 4A mutants (green traces) with  $\beta 2a$  (left) or  $\beta 2c$  (right). **(C)** Steady-state inactivation ( $r_{100}$ ) was measured at +10 mV. **(D)** Current inactivation was measured during 500-ms test pulses to +10 mV in cells expressing  $\alpha 1B$  WT (black traces) and 4A mutants (green traces) with  $\beta 2a$  (left) or  $\beta 2c$  (right) and 100 nM DiC8. **(E)**  $PIP_2$  depletion was measured during 500-ms test pulses to +10 mV in cells expressing  $\alpha 1B$  WT (black traces) and 4A mutants (green traces) with  $\beta 2a$  (left) or  $\beta 2c$  (right) and 100 nM DiC8. **(F)** Steady-state activation ( $G/G_{max}$ ) was measured during 500-ms test pulses to various voltages in cells expressing  $\alpha 1B$  WT (black traces) and 4A mutants (green traces) with  $\beta 2a$  (left) or  $\beta 2c$  (right). **(G)** Steady-state activation ( $V_{1/2}$ ) was measured during 500-ms test pulses to various voltages in cells expressing  $\alpha 1B$  WT (black traces) and 4A mutants (green traces) with  $\beta 2a$  (left) or  $\beta 2c$  (right). **Figure 5 continued on next page**

Figure 5 continued

$\beta$ 2c (right) subunits. (C) Summary of current inactivation of  $\text{Ca}_v2.2$  WT (black bars) and 4A (red bars) with  $\beta$ 2 subunits ( $n = 8-11$ ).  $r_{100}$  indicates the fraction of current remaining after 100-ms depolarization to +10 mV. (D) Current inhibition by Dr-VSP-mediated  $\text{PIP}_2$  depletion in cells expressing  $\text{Ca}_v2.2$  WT and 4A with the  $\beta$ 2a (left) or  $\beta$ 2c subunit (right).  $\text{Ca}_v2.2$  currents before (a) and after (b) the depolarizing pulse to +120 mV are superimposed in control (top) and Dr-VSP-expressing (bottom) cells. Peak tail current is indicated by arrowheads (trace a, black head; trace b, red head). (E) Summary of current inhibition (%) of  $\text{Ca}_v2.2$  WT (black bars) and 4A (red bars) by  $\text{PIP}_2$  depletion in control ( $n = 10$ ) and Dr-VSP-transfected cells ( $n = 8-12$ ). (F) The voltage dependence of normalized steady-state activation ( $G/G_{\text{max}}$ ) for  $\alpha$ 1B WT (black) and 4A mutants (green) with  $\beta$ 2a (left) or  $\beta$ 2c (right) subunits. Tail currents elicited between -40 and +40 mV in 10 mV steps, from a holding potential of -80 mV were normalized to the largest tail current in each series of test pulse. The curves were fitted by a Boltzmann function. Dashed line indicates the  $V_{1/2}$  of normalized steady-state activation. (G) Summary of the  $V_{1/2}$  of normalized steady-state activation in cells expressing  $\alpha$ 1B WT (black bars) and 4A mutants (green bars) with  $\beta$ 2a (upper) or  $\beta$ 2c (bottom) subunits ( $n = 7-10$ ). Dots indicate the individual data points for each cell. Data are mean  $\pm$  standard error of the mean (SEM). \*\* $p < 0.01$ , \*\*\* $p < 0.001$ , using two-way analysis of variance (ANOVA) followed by Sidak post hoc test.

The online version of this article includes the following source data and figure supplement(s) for figure 5:

**Source data 1.** Current inactivation ( $r_{100}$ ) and current inhibition (%) by  $\text{PIP}_2$  depletion in cells expressing  $\alpha$ 1B WT and 4A mutants with  $\beta$ 2a and  $\beta$ 2c.

**Figure supplement 1.** Sequence alignment of the C-terminal end of the I-II loop in  $\text{Ca}_v$   $\alpha$ 1 subunits.

**Figure supplement 2.** Current inactivation and  $\text{PIP}_2$  sensitivity of mutant  $\text{Ca}_v2.2$  channels with Lyn- $\beta$ 2c and Lyn-48aa- $\beta$ 2c.

**Figure supplement 2—source data 1.** Current inactivation ( $r_{100}$ ) and current inhibition (%) by  $\text{PIP}_2$  depletion in  $\text{Ca}_v2.2$  channels with Lyn- $\beta$ 2c and Lyn-48aa- $\beta$ 2c.

**Figure supplement 3.** Neutralization of polybasic residues in the distal end of the I-II loop domain plays a crucial role in determining current inactivation and  $\text{PIP}_2$  sensitivity of  $\text{Ca}_v2.2$  channels with  $\beta$ 2c.

**Figure supplement 3—source data 1.** Current inactivation ( $r_{100}$ ) and current inhibition (%) by  $\text{PIP}_2$  depletion in cells expressing WT  $\alpha$ 1B,  $\alpha$ 1B R465,466A, and  $\alpha$ 1B R476,477A with  $\beta$ 2a and  $\beta$ 2c.

for Dr-VSP-induced channel modulation, current suppression was much weaker in  $\alpha$ 1C-1B 4A channels with  $\beta$ 2c than in  $\alpha$ 1C-1B WT with  $\beta$ 2c (Figure 6B, C). We confirmed that the current suppression by  $\text{M}_1\text{R}$  activation were not recovered in both  $\alpha$ 1C-1B WT and  $\alpha$ 1C-1B 4A channels by a prepulse regardless of the coupled  $\beta$ 2 isotypes (Figure 6D, E). We additionally used  $\text{G}_i$ -coupled  $\text{M}_2$  muscarinic receptor ( $\text{M}_2\text{R}$ ) to further examine whether the polybasic motif in I-II loop affects the  $\text{G}\beta\gamma$ -mediated modulation of  $\text{Ca}_v2.2$  channels (Figure 6—figure supplement 1).  $\text{M}_2\text{R}$  activation inhibited the currents evoked by a +10-mV test pulse without significant difference between WT and 4A  $\alpha$ 1B with  $\beta$ 2a or  $\beta$ 2c (Figure 6—figure supplement 1B, C).  $\text{M}_2\text{R}$  activation commonly slowed down the activation kinetics of  $\text{Ca}_v2.2$  currents (Figure 6—figure supplement 1D). We have previously reported that subcellular localization of the  $\text{Ca}_v$   $\beta$  subunit plays important roles in determining the  $\text{G}\beta\gamma$ -dependent inhibition of  $\text{Ca}_v2.2$  channels; membrane-anchored  $\beta$ 2a subunit changes  $\text{Ca}_v2.2$  channels are more sensitive to  $\text{G}\beta\gamma$ -mediated voltage-dependent inhibition, whereas cytosolic  $\beta$ 2b and  $\beta$ 3 subunit changes channels are less sensitive to  $\text{G}\beta\gamma$ -mediated voltage-dependent inhibition (Keum et al., 2014). In  $\text{Ca}_v2.2$  channels with the  $\beta$ 2a subunit, the recoveries from  $\text{G}\beta\gamma$ -mediated inhibition did not significantly differ between WT  $\alpha$ 1B and 4A  $\alpha$ 1B (Figure 6—figure supplement 1E, F). However, in  $\text{Ca}_v2.2$  with the  $\beta$ 2c subunit, there was less recovery from  $\text{G}\beta\gamma$ -mediated inhibition in  $\alpha$ 1B WT than in  $\alpha$ 1B 4A (Figure 6—figure supplement 1E, F). Recovery from  $\text{M}_2\text{R}$ -mediated inhibition in 4A  $\alpha$ 1B with  $\beta$ 2c was similar to the values of WT and 4A  $\alpha$ 1B with  $\beta$ 2a (Figure 6—figure supplement 1E, F).

### **$\text{PIP}_2$ -binding site in $\text{S4}_{\text{II}}$ domain is important in maintaining the $\text{Ca}_v2.2$ channel activity regardless of the coupled $\beta$ 2 isotype**

Recently, the cryo-electron microscopic structure of human  $\text{Ca}_v2.2$  complex composed of  $\alpha$ 1B,  $\alpha$ 2 $\delta$ 1, and  $\beta$ 3 subunits was revealed at a resolution of 3.0 Å (Dong et al., 2021; Gao et al., 2021). These studies have shown that the 5-phosphate group of membrane  $\text{PIP}_2$  interacts with two basic residues (R584 and K587) within  $\text{S4}_{\text{II}}$  domain of  $\alpha$ 1B. We examined whether the two basic residues affect the  $\text{PIP}_2$  sensitivity of  $\text{Ca}_v2.2$  channels. First, we constructed neutralized mutant  $\alpha$ 1B subunits in which the two basic residues in  $\text{S4}_{\text{II}}$  were replaced by alanine residues ( $\alpha$ 1B RA/KA) (Figure 7A). In  $\text{Ca}_v2.2$  channels with  $\beta$ 2a, the inactivation kinetics of the current were not changed in  $\alpha$ 1B and  $\alpha$ 1B RA/KA, regardless of the 4A mutation (Figure 7B, C). In  $\text{Ca}_v2.2$  with  $\beta$ 2c, WT  $\alpha$ 1B RA/KA showed faster inactivation than WT  $\alpha$ 1B, whereas 4A  $\alpha$ 1B RA/KA showed much slower but similar inactivation to those of  $\alpha$ 1B and  $\alpha$ 1B RA/KA with  $\beta$ 2a (Figure 7B, C). Additionally, the effects of  $\text{PIP}_2$  depletion on current amplitude were

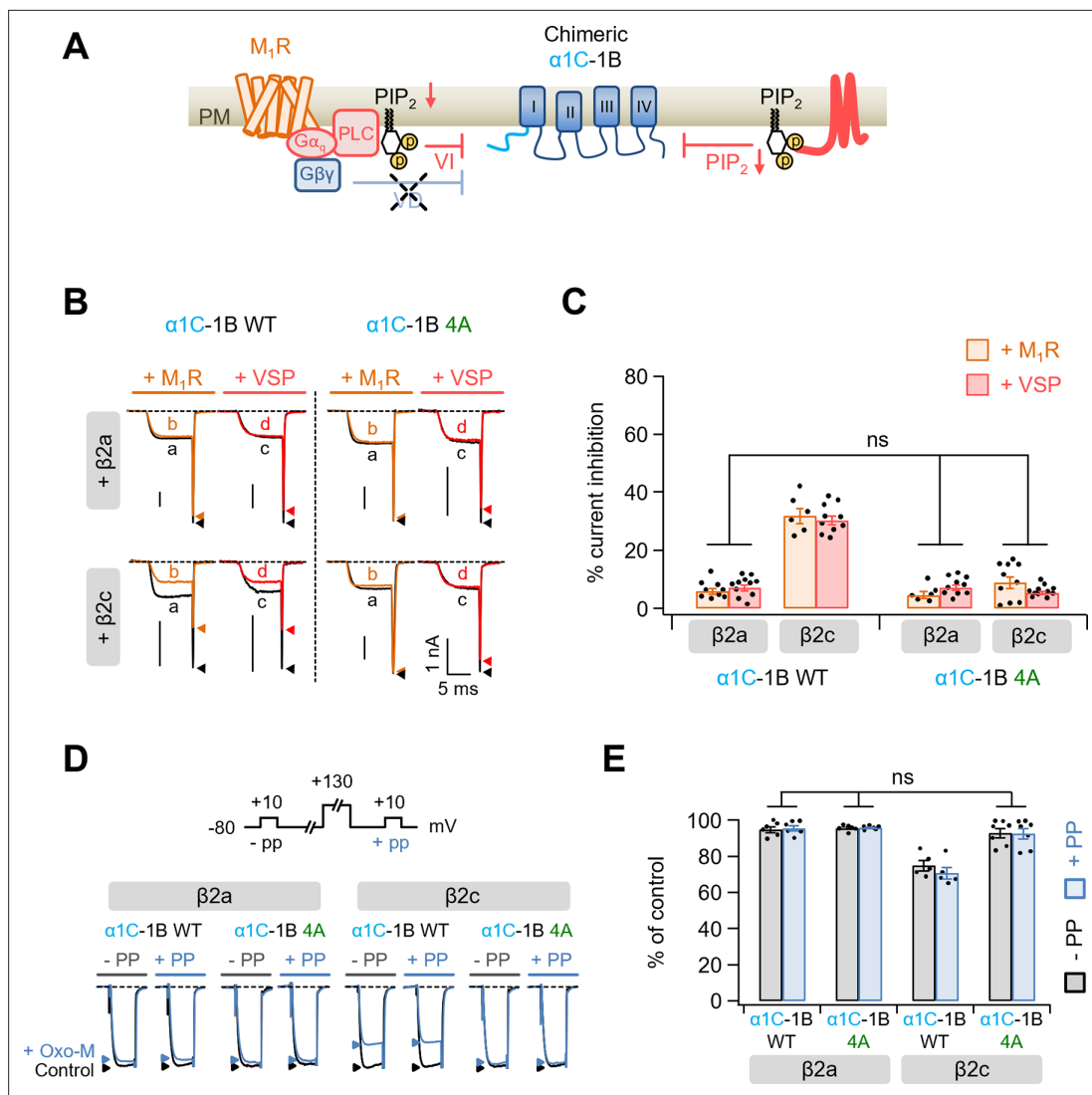


**Figure 6.** Modulation by M<sub>1</sub> muscarinic stimulation and Dr-VSP activation in Gβγ-insensitive chimeric α1C-1B Ca<sub>v</sub>2.2 channel. **(A)** Schematic diagram showing the inhibitory signaling from M<sub>1</sub> muscarinic acetylcholine receptor (M<sub>1</sub>R) and Dr-VSP to Gβγ-insensitive chimeric α1C-1B channel. VI, voltage-independent inhibition; VD, voltage-dependent inhibition. **(B)** Current traces before (a, black) and during (b, orange) the 10 μM Oxo-M application or before (c, black) and after (d, red) the Dr-VSP activation in cells expressing the α1C-1B WT and α1C-1B 4A with β2a or β2c subunits. Peak tail current is indicated by arrowheads (trace a, black head; trace b, orange head; trace c, black head; trace d, red head). **(C)** Summary of current inhibition (%) of α1C-1B WT and α1C-1B 4A by M<sub>1</sub>R stimulation (orange bars) or Dr-VSP activation (red bars) in cells with β2a or β2c subunits (n = 6–11). **(D)** Current traces before (control, black) and during the Oxo-M application (+Oxo-M, blue) were superimposed. Cells were given a test pulse (-PP) and then depolarized to +130 mV, followed by the second test pulse after 20 ms (+PP). Peak current is indicated by arrowheads (control, black head; +Oxo-M, blue head). **(E)** Summary of the prepulse experiments in before and Oxo-M perfused cells with α1C-1B WT and α1C-1B 4A with β2a or β2c subunits (n = 5–7). The current amplitude after Oxo-M application is given as percentage of the initial control. Dots indicate the individual data points for each cell. Data are mean ± standard error of the mean (SEM).

The online version of this article includes the following source data and figure supplement(s) for figure 6:

**Source data 1.** Current inhibition (%) of α1C-1B WT and 4A mutants by M<sub>1</sub>R or Dr-VSP activation in cells expressing with β2a and β2c.

**Figure supplement 1.** Polybasic motif at the C-terminal end of the I–II loop affects in determining the M<sub>2</sub> muscarinic modulation of Ca<sub>v</sub>2.2 channels.

**Figure supplement 1—source data 1.** Current inhibition (%) of α1B WT and 4A mutants by M<sub>2</sub>R activation in cells expressing with β2a and β2c.

measured in these mutant channels. Mutation of the two basic residues in S4<sub>II</sub> completely abolished the Dr-VSP-mediated current inhibition in cells expressing WT α1B RA/KA or 4A α1B RA/KA with the β2a subunit, while there was approximately 5% inhibition in cells expressing WT and 4A α1B with β2a (**Figure 7D, E**). Importantly, PIP<sub>2</sub> depletion significantly inhibited the currents in cells expressing WT

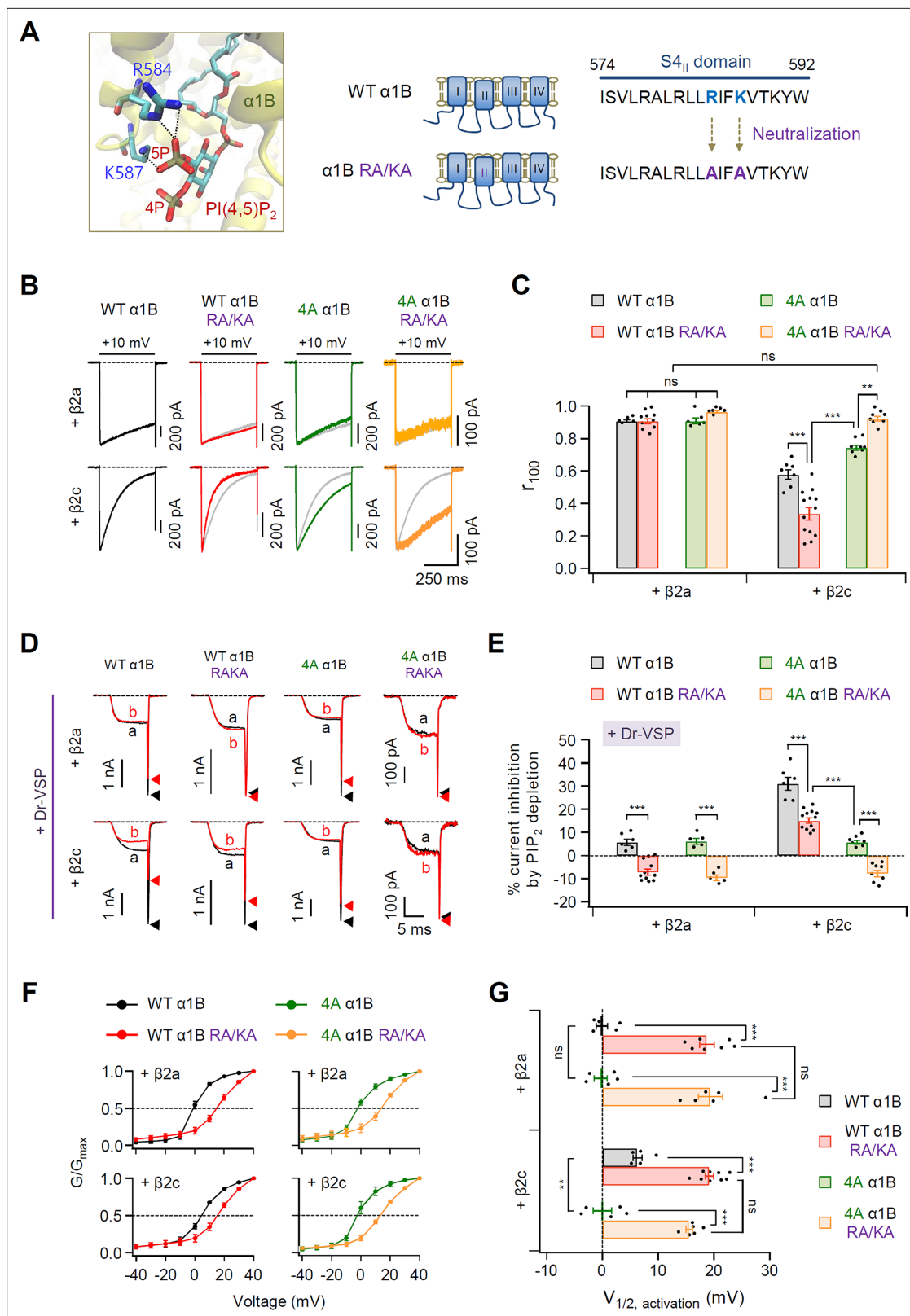


**Figure 7.** PIP<sub>2</sub>-binding residues within the S<sub>4II</sub> domain plays an important role in determining steady-state activation and PIP<sub>2</sub> sensitivity of Ca<sub>v</sub>2.2 channels. **(A)** Distance analysis of PIP<sub>2</sub>-binding site in the S<sub>4II</sub> domain of α<sub>1B</sub> subunit. Two amino acids (R584 and K587) interacting with the 5-phosphate of PIP<sub>2</sub> were neutralized to alanine residues (RA/KA). **(B)** Current inactivation was measured during 500-ms test pulses to +10 mV in cells expressing WT α<sub>1B</sub> (black traces), WT α<sub>1B</sub> RA/KA (red traces), 4A α<sub>1B</sub> (green traces), and 4A α<sub>1B</sub> RA/KA (orange traces) with β<sub>2a</sub> (upper) or β<sub>2c</sub> (bottom). Gray traces

Figure 7 continued on next page

Figure 7 continued

present the curve of WT  $\alpha 1B$  for comparison. (C) Summary of current inactivation of  $Ca_v2.2$  channel in cells expressing indicated  $\alpha 1B$  with  $\beta 2a$  ( $n = 5-10$ ) or  $\beta 2c$  ( $n = 7-13$ ). The  $r_{100}$  indicates the fraction of current remaining after 100-ms depolarization to +10 mV. (D) Current inhibition by Dr-VSP-mediated  $PIP_2$  depletion in cells expressing WT  $\alpha 1B$ , WT  $\alpha 1B$  RA/KA, 4A  $\alpha 1B$ , and 4A  $\alpha 1B$  RA/KA with  $\beta 2a$  (upper) or  $\beta 2c$  (bottom) subunits.  $Ca_v2.2$  currents before (a) and after (b) the depolarizing pulse to +120 mV are superimposed in Dr-VSP-expressing cells. Peak tail current is indicated by arrowheads (trace a, black head; trace b, red head). (E) Summary of the  $Ca_v2.2$  current inhibition (%) by  $PIP_2$  depletion in cells expressing indicated  $\alpha 1B$  with  $\beta 2a$  ( $n = 6-12$ ) or  $\beta 2c$  ( $n = 5-11$ ). (F) The voltage dependence of normalized steady-state activation ( $G/G_{max}$ ) for WT  $\alpha 1B$  (black), WT  $\alpha 1B$  RA/KA (red), 4A  $\alpha 1B$  (green), and 4A  $\alpha 1B$  RA/KA (orange) with  $\beta 2a$  (left) or  $\beta 2c$  (right). Tail currents elicited between -40 and +40 mV in 10 mV steps, from a holding potential of -80 mV were normalized to the largest tail current in each series of test pulse. The curves were fitted by a Boltzmann function. Dashed line indicates the  $V_{1/2}$  of normalized steady-state activation. (G) Summary of the  $V_{1/2}$  of normalized steady-state activation in F ( $n = 5-9$ ). Dots indicate the individual data points for each cell. Data are mean  $\pm$  standard error of the mean (SEM). \*\* $p < 0.01$ , \*\*\* $p < 0.001$ , using two-way analysis of variance (ANOVA) followed by Sidak post-hoc test.

The online version of this article includes the following source data and figure supplement(s) for figure 7:

**Source data 1.** Current inactivation ( $r_{100}$ ), current inhibition (%) by  $PIP_2$  depletion and the  $V_{1/2}$  of normalized steady-state activation in cells expressing WT  $\alpha 1B$ , WT  $\alpha 1B$  RA/KA, 4A  $\alpha 1B$ , and 4A  $\alpha 1B$  RA/KA with  $\beta 2a$  or  $\beta 2c$ .

**Figure supplement 1.**  $PIP_2$  sensitivity of  $\alpha 1B$  R578,581A with  $\beta 2a$  or  $\beta 2c$  subunits.

**Figure supplement 1—source data 1.** Current inhibition (%) by  $PIP_2$  depletion in cells expressing WT  $\alpha 1B$  and  $\alpha 1B$  R578,581A with  $\beta 2a$  or  $\beta 2c$ .

$\alpha 1B$  RA/KA and  $\beta 2c$ , whereas 4A  $\alpha 1B$  RA/KA exhibited no current inhibition, like  $\alpha 1B$  RA/KA with  $\beta 2a$  (Figure 7D, E). Since the mutation of two basic residues changes the gating charges of  $S4_{II}$  voltage-sensor domain, we additionally tested if other charge residues within the  $S4_{II}$  similarly affects  $PIP_2$  sensitivity of  $Ca_v2.2$  channels. We eliminated two adjacent arginine residues (R578 and R581) in  $S4_{II}$  by replacing with alanine ( $\alpha 1B$  R578,581A) (Figure 7—figure supplement 1A). In both WT  $\alpha 1B$  and  $\alpha 1B$  R578,581A channels with  $\beta 2a$  or  $\beta 2c$ , there was no significant changes in the current inhibition by  $PIP_2$  depletion (Figure 7—figure supplement 1B, C), suggesting that the R578 and R581 charge residues near the  $PIP_2$ -binding pocket were not involved in the  $PIP_2$  interaction. Next, we examined the functional role of the  $PIP_2$ -binding site within  $S4_{II}$  in the voltage-dependent activation of  $Ca_v2.2$  channels. Regardless of  $\beta 2$  isotype, the activation curves were significantly shifted toward the depolarization direction in both WT  $\alpha 1B$  RA/KA and 4A  $\alpha 1B$  RA/KA (Figure 7F, G). Together, our results suggest that the two basic residues within the  $S4_{II}$  domain consistently interact with  $PIP_2$  regardless of the coupled  $\beta 2$  isotype. Additionally,  $PIP_2$ -binding to the  $S4_{II}$ -binding pocket is important in maintaining stable  $Ca_v2.2$  channel gating.

## Discussion

This study has expanded our understanding of the inter-regulatory actions of the  $Ca_v$   $\beta$  subunit and membrane  $PIP_2$  on  $Ca_v$  channel gating properties, including inactivation kinetics, current density, and voltage dependency. Our data predict that  $Ca_v2.2$  channels complexed with any  $\beta$  isotype can interact with membrane  $PIP_2$  through the binding pocket in the  $S4_{II}$  domain (Figure 8). However, in  $Ca_v2.2$  channels with cytosolic  $\beta 2c$ , there seems to be another interaction with  $PIP_2$  through the nonspecific phospholipid-binding site at the distal end of the  $\alpha 1B$  I-II loop. This leads to the channel becoming highly sensitive to Dr-VSP-mediated  $PIP_2$  depletion (Figure 8, lower panel). In channels with  $\beta 2a$ , the membrane anchoring of the subunit may interfere with the interaction between the phospholipid-binding site and  $PIP_2$ . This converts the channels to a less  $PIP_2$ -sensitive state (Figure 8, upper panel). Additionally, the neutralization of polybasic residues in the I-II loop to alanine abolished  $PIP_2$  binding on the phospholipid-binding site regardless of  $\beta$  isotype, which led to the less  $PIP_2$ -sensitive state (Figure 8, 4A  $\alpha 1B$ ). By contrast, the neutralization of two basic residues in the  $S4_{II}$ -binding pocket slightly reduced  $PIP_2$  sensitivity in channels with cytosolic  $\beta 2c$  subunits and completely abolished the response in channels with a  $\beta 2a$  subunit (Figure 8,  $\alpha 1B$  RA/KA). Taken together, these data showed that when  $PIP_2$  molecules were depleted at the  $VSD_{II}$   $PIP_2$  and polybasic phospholipid-binding sites or both sites were mutated to neutralized amino acid residues, the channels move to a nonconducting state (Figure 8, 4A  $\alpha 1B$  RA/KA).

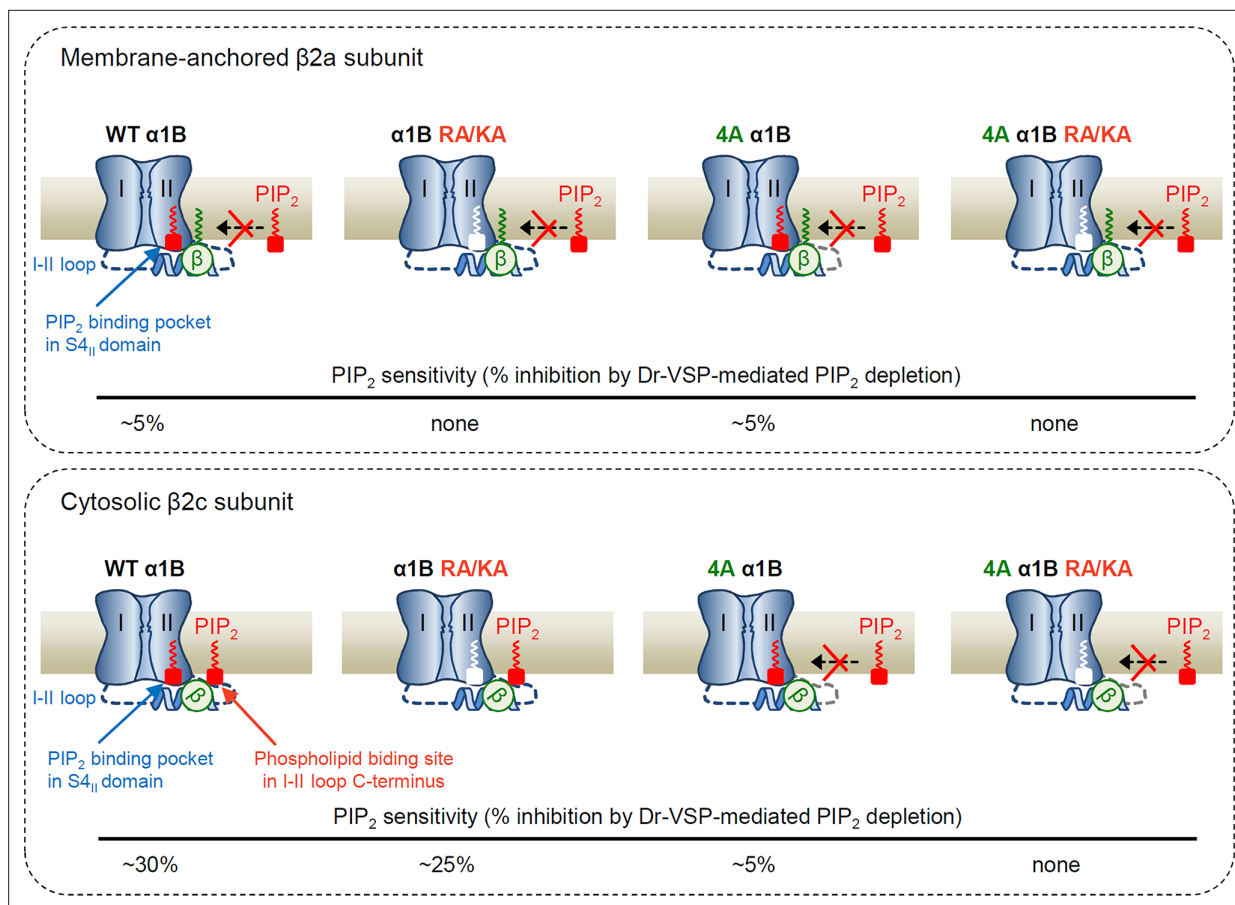


**Figure 8.** Schematic model showing the differential regulation of  $\text{Ca}_v2.2$  channels with membrane-anchored and cytosolic  $\beta$  subunits by  $\text{PIP}_2$ . The channel possesses two distinct  $\text{PIP}_2$ -interacting sites: the  $\text{PIP}_2$ -binding pocket in the  $\text{S4}_{II}$  domain and the nonspecific phospholipid-binding site in the I-II loop C-terminus. When the  $\text{Ca}_v2.2$  channel is coupled with membrane-anchored  $\beta$ 2a (upper panel), the proximal interaction of N-terminus of  $\beta$ 2a with plasma membrane (PM) via its lipid anchor eliminates the binding of  $\text{PIP}_2$  to the polybasic phospholipid site on I-II loop, leading to the state less sensitive to  $\text{PIP}_2$  (upper left). In this condition, mutation of the  $\text{PIP}_2$ -interacting phospholipid site in the I-II loop does not change the  $\text{PIP}_2$  sensitivity (upper 4A  $\alpha$ 1B). In contrast, when the  $\text{Ca}_v2.2$  channel is coupled with cytosolic  $\beta$ 2c (lower panel), there is no interaction of  $\beta$  subunit with the PM, leading to the higher  $\text{PIP}_2$ -sensitive state through the association of the polybasic phospholipid-binding site with acid phospholipids in the PM (lower left). In 4A mutant channels,  $\text{PIP}_2$  interaction with the phospholipid-binding site is abolished, changing the channels to a state that shows only  $\text{PIP}_2$  binding to the binding pocket in  $\text{S4}_{II}$  domain.  $\text{PIP}_2$  depletion in the PM or mutations of both  $\text{PIP}_2$ -interacting sites alter channels to the nonconducting state by shifting the voltage-dependent activation to the depolarization direction (lower right). The approximate  $\text{PIP}_2$  sensitivity of each channel state in response to Dr-VSP activation is indicated as % inhibition at the bottom of each panel.

### $\text{Ca}_v$ $\beta$ subunits regulate bidentate $\text{PIP}_2$ binding to $\text{Ca}_v2.2$ channels

Previous studies have proposed a bidentate model for the  $\text{PIP}_2$  modulation of N-type  $\text{Ca}_v2.2$  channel regulation (Heneghan et al., 2009; Hille et al., 2015; Mitra-Ganguli et al., 2009; Roberts-Crowley and Rittenhouse, 2009). In this model, lipidation on the N-terminus of  $\text{Ca}_v$   $\beta$  subunits disrupts the hydrophobic interaction between the two fatty acyl chains of  $\text{PIP}_2$  and  $\text{Ca}_v2.2$  channels, and thus reduces current inhibition by  $\text{PIP}_2$  depletion. For example,  $\beta$ 2a subunits interact with the PM through two palmitoyl fatty acyl chains in the N-terminus, leading to competition in binding to  $\text{Ca}_v$  channels with the fatty side chains of  $\text{PIP}_2$ . This competition removes  $\text{PIP}_2$  from the channel-binding site. Thus,  $\text{Ca}_v$  channels with  $\beta$ 2a are uncoupled from the membrane  $\text{PIP}_2$  and show lower  $\text{PIP}_2$  sensitivity to  $\text{PIP}_2$  depletion. By contrast, non-lipidated  $\beta$ 3 subunits expressed in the cytosol do not interrupt the interaction between the fatty acyl chains of  $\text{PIP}_2$  and  $\text{Ca}_v2.2$  channels, and show high  $\text{PIP}_2$  sensitivity of channels (Heneghan et al., 2009; Hille et al., 2015; Suh et al., 2012). Consistently, we found that when the  $\beta$ 3 subunits were anchored to the PM by adding the lipidation signal of Lyn to the N-terminus, the engineered Lyn- $\beta$ 3 construct decreased the  $\text{PIP}_2$  sensitivity of  $\text{Ca}_v2.2$  channels, similar to  $\beta$ 2a. The Lyn<sub>11</sub> domain incorporates into the PM through the G2-myristoylated and C3-palmitoylated lipid anchors;



therefore, Lyn- $\beta$ 3 mimics  $\beta$ 2a in competing with PIP<sub>2</sub> for the hydrophobic Ca<sub>v</sub>2.2 channel interaction. Conversely, the lipid anchor of Lyn-48aa- $\beta$ 2c may be localized far from the channel complex because of its long N-terminal flexible linker, suggesting that these mutant subunits cannot disrupt the hydrophobic interaction between PIP<sub>2</sub> and channels.

Our results provide advance information about the bidentate model. First, we confirmed that two distinct PIP<sub>2</sub>-interacting sites were preserved in the Ca<sub>v</sub>2.2 channel: the binding pocket in VSD<sub>II</sub> and phospholipid-binding site in the I-II loop. Our data are consistent with that the 5-phosphate group of membrane PIP<sub>2</sub> interacts with the two basic residues within the S4<sub>II</sub> domain of Ca<sub>v</sub>2.2 channels regardless of  $\beta$ 2 isotype. The additional interaction of PIP<sub>2</sub> with the nonspecific phospholipid binding site in the distal I-II loop of Ca<sub>v</sub> channels was mainly observed in Ca<sub>v</sub>2.2 channels with the cytosolic Ca<sub>v</sub>  $\beta$ 2c subunit. Our data indicate that PIP<sub>2</sub>-binding to the I-II loop phospholipid-binding site is selectively disrupted by the lipid anchor of membrane-anchored  $\beta$ 2a. The hydrophobic interaction of the palmitoyl or myristoyl groups of Ca<sub>v</sub>  $\beta$ 2a or Lyn- $\beta$  constructs with channel complex may be the cause of PIP<sub>2</sub> release from the lower-affinity I-II loop phospholipid-binding site (**Roberts-Crowley and Rittenhouse, 2009**). When PIP<sub>2</sub> interacts with the VSD<sub>II</sub> PIP<sub>2</sub>-binding site of Ca<sub>v</sub>2.2 channels complexed with  $\beta$ 2a, the PIP<sub>2</sub> sensitivity of the channels dramatically decreased to approximately 5%. Our results suggested that this minimal PIP<sub>2</sub> sensitivity specifically caused by PIP<sub>2</sub> degradation on VSD<sub>II</sub>-binding pocket by Dr-VSP activation.

This work suggests that the PIP<sub>2</sub> sensitivity of the Ca<sub>v</sub>2.2 channel is mainly affected by the length between the lipid anchor and GK domain of the Ca<sub>v</sub>  $\beta$  subunit. Although both Lyn- $\beta$ 2c and Lyn-48aa- $\beta$ 2c are localized at the PM, the PIP<sub>2</sub> sensitivity and inactivation kinetics of Ca<sub>v</sub>2.2 channels are significantly different from each other: Ca<sub>v</sub>2.2 channels with Lyn- $\beta$ 2c subunits exhibited relatively slower inactivation kinetics and lower PIP<sub>2</sub> sensitivity, similar to channels with the membrane-anchored  $\beta$ 2a subunit. By contrast, Ca<sub>v</sub>2.2 channels with Lyn-48aa- $\beta$ 2c subunits exhibited faster inactivation kinetics and higher PIP<sub>2</sub> sensitivity, similar to channels with the cytosolic  $\beta$ 2c subunit. Similarly, disruption of the SH3-GK interaction in the membrane-anchored  $\beta$ 2a subunit accelerated current inactivation and increased the current inhibition by PIP<sub>2</sub> depletion. Moreover, real-time translocation of the lipid anchor, Lyn<sub>11</sub>, to the channel complex by rapamycin-inducible dimerization systems slowed the inactivation and decreased the PIP<sub>2</sub> sensitivity of Ca<sub>v</sub>2.2 channels. Inversely, incremental increases in flexible linker length between the lipid anchor and GK domain of Ca<sub>v</sub>  $\beta$ 2 subunits gradually accelerated the inactivation kinetics and increased the PIP<sub>2</sub> sensitivity of Ca<sub>v</sub>2.2 channels. However, the mechanism by which the physical distance from the PM lipid to GK domain of the Ca<sub>v</sub>  $\beta$  subunit affects the PIP<sub>2</sub> sensitivity of the Ca<sub>v</sub>2.2 channel is not fully understood yet. Another possibility is that torsional rigidity of the linker domain may be different depending on the length and thus differently restrict the cytoplasmic movement of Ca<sub>v</sub>  $\beta$  subunit as well as the gating of Ca<sub>v</sub>2.2 channels.

Colecraft et al. have reported that chemically induced anchoring of intracellular loops of the channels to the PM can modulate the gating of the HVA Ca<sup>2+</sup> channel (**Subramanyam and Colecraft, 2015; Yang et al., 2013**). They have shown that PdBu-induced translocation to the PM of chimeric  $\beta$ 3-C1<sub>PKC $\gamma$</sub> , which is assembled by fusing the C1 domain of PKC $\gamma$  to the C-terminus of the  $\beta$ 3 subunit, leads to the inhibition of the Ca<sub>v</sub>2.2 current. Conversely, the C1<sub>PKC $\gamma$</sub> - $\beta$ 3 subunit, which is assembled by adding C1<sub>PKC $\gamma$</sub>  to the N-terminus of the  $\beta$ 3 subunit, has no effect on the current (**Yang et al., 2013**). These studies suggest that the polarity of the PM-targeting domain may play an important role in determining the Ca<sub>v</sub>2.2 channel gating; however, the molecular basis of the differential regulation mechanism remain unclear. On the basis of our results, we speculate that the C1<sub>PKC $\gamma$</sub> - $\beta$ 3 form may be insufficient to disrupt the interaction with between phospholipid-binding site and PIP<sub>2</sub> in Ca<sub>v</sub>2.2 channels because the length from the C1<sub>PKC $\gamma$</sub>  and the GK domain of the  $\beta$ 3 subunit is 175 aa. This could be too long to interfere the interaction between PIP<sub>2</sub> and Ca<sub>v</sub>2.2 channels.

Recently, **Gao et al., 2021** have shown that two basic gating charge residues (R584 and K587) within the S4<sub>II</sub> domain of human Ca<sub>v</sub>2.2 channel interact with the 5-phosphate group of membrane PIP<sub>2</sub>. In our present work, we found that mutation of the two residues (RA/KA) in the S4<sub>II</sub> domain completely blocked the Dr-VSP-induced current suppression in channels with  $\beta$ 2a and shifted the voltage-dependent activation curve toward the depolarization direction regardless of Ca<sub>v</sub>  $\beta$ 2 isotype. The cryo-EM structure does not show the nonspecific PIP<sub>2</sub>-binding site in the channels probably because it is located in the flexible I-II loop. We hypothesize that the polybasic residues in the I-II loop tether to the anionic phospholipids through the electrostatic interaction and this dipole-dipole

interaction may contribute to the low-affinity phospholipid-binding site (Yeon *et al.*, 2018). In contrast, the VSD<sub>II</sub> PIP<sub>2</sub>-binding site forms a pocket-like structure inside the S4<sub>II</sub> domain and covered by the AID domain in the cytosolic side (Dong *et al.*, 2021; Gao *et al.*, 2021), which could stabilize the domain in a high-affinity PIP<sub>2</sub> interacting site. Thus, it is possible that the PIP<sub>2</sub> molecule inside the VSD<sub>II</sub> PIP<sub>2</sub>-binding pocket is relatively less accessible to the degradation by phospholipase C or Dr-VSP, leading to the lower PIP<sub>2</sub> sensitivity in Ca<sub>v</sub>2.2 channels.

In conclusion, our findings provide new insights on the regulatory mechanism of Ca<sub>v</sub>2.2 channel gating by Ca<sub>v</sub> β subunits. Our recent study has reported that when intracellular Ca<sup>2+</sup> is increased by depolarizing the cells or activating G<sub>q</sub>-coupled receptors, the high intracellular Ca<sup>2+</sup> concentration induces a dissociation of the N-terminus of the Ca<sub>v</sub> β2e subunit from the PM. This increases both the inactivation kinetics and PIP<sub>2</sub> sensitivity of Ca<sub>v</sub>2.2 channels (Kim *et al.*, 2016). The N-terminus of the β2e subunit is anchored to the PM via electrostatic interaction with the anionic phospholipids of these PM. These studies suggest that dissociation of the β2e subunit from the membrane leads to an interaction between the I-II loop phospholipid-binding site and PIP<sub>2</sub>, which changes the gating properties of Ca<sub>v</sub> channels in physiological conditions. The interaction of Ca<sub>v</sub> α1B with β subunits can be dynamically exchanged by other free β isoforms in intact cells (Yeon *et al.*, 2018); therefore, the displacement of cytosolic β subunits by membrane-tethered β subunits on Ca<sub>v</sub> channels will abolish the interaction with between PIP<sub>2</sub> and the I-II loop phospholipid-binding site via lipid anchor of membrane-tethered β subunits, which alters the Ca<sub>v</sub> channel gating properties. Further studies are needed to investigate whether the conformational shift of the I-II loop to the membrane or cytosolic face by endogenous β subunit combinations determines Ca<sub>v</sub> channel gating in neurons and other excitable cells.

## Materials and methods

### Cell culture and transfection

Human embryonic kidney tsA-201 cells (large T-antigen transformed HEK293 cells; RRID:CVCL\_2737) were a kind gift from Dr Bertil Hille at University of Washington. The identity of this cell line has been authenticated by STR analysis and has recurrently tested negative for mycoplasma contamination using PCR (Cosmogenetech, Daejeon, South Korea). Cells were maintained in Dulbecco modified Eagle medium (Invitrogen, CA) supplemented with 10% fetal bovine serum (Invitrogen, CA) and 0.2% penicillin/streptomycin (Invitrogen, CA) in 100 mm culture dishes at 37°C with 5% CO<sub>2</sub>. The cells were transiently transfected with Lipofectamine 2000 (Invitrogen, CA) when the confluency of the cells reached 50–70%. For assessment of Ca<sub>v</sub> channel expression, the cells were co-transfected with α1 of Ca<sub>v</sub>, α2δ1, and various β2 chimera constructs in a 1:1:1 molar ratio. The transfected cells were plated onto a coverslip chip coated with poly-L-lysine (0.1 mg/ml, Sigma-Aldrich, MO) 24–36 hr after transfection. Plated cells were used for electrophysiological and confocal experiment within 24 hr after plating, as described previously (Park *et al.*, 2017).

### Plasmids

The following plasmids were used: The calcium channel subunits α1B of rat Ca<sub>v</sub>2.2e[37b] (GenBank Sequence accession number AF055477) and rat α2δ1 (AF286488) were from Diane Lipscombe, Brown University, Providence, RI. Chimeric α1C-1B was generously donated by David T. Yue, Johns Hopkins University, Baltimore, MD. Mouse cDNAs of β2a and β2c were generously donated by Veit Flockerzi, Saarland University, Homburg, Germany. The Dr-VSP (AB308476) was obtained from Yasushi Okamura, Osaka University, Osaka, Japan.

### Molecular cloning

Cloning of β2a-GFP, β2a(C3,4S)-GFP, and β2c-GFP was performed as previously described (Park *et al.*, 2017). For the generation of various β2 chimera constructs, we used the one-step sequence- and ligation-independent cloning (SLIC) as a time-saving and cost-effective cloning strategy (Jeong *et al.*, 2012). First, pEGFP-N1, pEYFP-N1, and mCherry-N1 vectors (Clontech) were linearized by KpnI restriction enzyme digestion. The cDNAs encoding β2a, β2c, Lyn, FRB, or FKBP were amplified by PCR using primers with an 18-bp homologous sequence attached to each end of the linearized vector. Primers used for β2 chimera constructs are listed in **Supplementary file 1**. Second, the linearized vector and PCR fragments were blended and incubated at room temperature for 2.5 min with T4

DNA polymerase (NEB, The Netherlands). Third, the DNA mixture was kept on ice for 10 min, after which competent *Escherichia coli* cells were transformed directly. For the deletion and point mutation of GK-SH3 interaction sites of the  $\beta 2$  subunit and the potential PIP<sub>2</sub>-interaction sites of  $\alpha 1B$ , first, the  $\alpha 1B$  or  $\beta 2$  subunits were amplified by inverse PCR using nPfu-special DNA polymerase (Enzymomics, Daejeon, South Korea). Second, the PCR product was 5'-phosphorylated by T4 polynucleotide kinase (Enzymomics, Daejeon, South Korea) and plasmid DNA was digested by Dpn I (Agilent Technologies, Santa Clara, CA). Finally, the PCR product was ligated by T4 DNA ligase (NEB, The Netherlands). The primers used for mutagenesis are listed in **Supplementary file 2**. All the chimera and mutant constructs were verified by DNA sequencing (Macrogen, South Korea).

## Electrophysiology

The whole-cell configuration of the patch-clamp technique was used to record Ba<sup>2+</sup> currents using HEKA EPC-10 patch-clamp amplifier with pulse software (HEKA Elektronik). Electrodes pulled from glass micropipette capillaries (Sutter Instrument) had resistances of 2–4 M $\Omega$ . The whole-cell access resistance was of 2–6 M $\Omega$ , and series resistance errors were compensated by 60%. For all recordings, cells were maintained at –80 mV. The external solution contained 10 mM BaCl<sub>2</sub>, 150 mM NaCl, 1 mM MgCl<sub>2</sub>, 10 mM HEPES, and 8 mM glucose, adjusted to pH 7.4 with NaOH and an osmolarity of 321–350 mOsm. The internal solution of the pipette consisted of 175 mM CsCl<sub>2</sub>, 5 mM MgCl<sub>2</sub>, 5 mM HEPES, 0.1 mM 1,2-bis(2-aminophenoc)ethane *N,N,N',N'*-tetraacetic acid (BAPTA), 3 mM Na<sub>2</sub>ATP, and 0.1 mM Na<sub>3</sub>GTP, adjusted to pH 7.4 with CsOH and an osmolarity of 321–350 mOsm.

## Confocal imaging

All imaging examinations were performed with an LSM 700 confocal microscope (Carl Zeiss AG) at room temperature (22–25°C). The external solution for confocal imaging contained 160 mM NaCl, 2.5 mM KCl, 2 mM CaCl<sub>2</sub>, 1 mM MgCl<sub>2</sub>, 10 mM HEPES, and 8 mM glucose, adjusted to pH 7.4 with NaOH and an osmolarity of 321–350 mOsm. For live-cell imaging, images were obtained by scanning cells with a  $\times 40$  (water) apochromatic objective lens at 1024  $\times$  1024 pixels using digital zoom. Analysis of line scanning of fluorescence images was performed using the 'profile' tool in Zen 2012 lite imaging software (Carl Zeiss Microimaging). To analyze colocalization, we performed quantitative colocalization analysis using Fiji software with the Colocalization Threshold plugin to determine the Pearson's correlation coefficient (*R*). Pixel intensities were presented as 2D intensity histograms with a linear regression line and as bar graphs with mean *R* values. All images were transferred from LSM4 to JPEG format.

## Förster resonance energy transfer

FRET experiments were performed using a monochromator (Polychrome V; TILL Photonics) with a  $\times 40$ , NA 0.95 dry immersion objective lens (Olympus). Regular pulses of indigo light (438  $\pm$  12 nm) excited the fluorescent proteins. Emission was separated into short (460–500 nm) and long (520–550 nm) wavelengths by appropriate filters and then acquired by two photomultipliers. Donor and acceptor signals obtained by photometry (TILL Photonics) were transferred to the data acquisition board (PCI-6221; National Instruments). Signal acquisition and real-time calculation of the FRET ratio were conducted by a custom program. The FRET ratio was calculated as follows:

$$\text{FRET}_r = (\text{YFP}_C - \text{cFactor} \times \text{CFP}_C) / \text{CFP}_C$$

CFP<sub>C</sub> is the CFP emission detected by the short-wavelength photomultiplier, and YFP<sub>C</sub> is the YFP emission detected by the long-wavelength photomultiplier, as described previously (*Keum et al., 2014*).

## Calculation of distance with a WLC model

The Lyn-Linker-(additional Link) structure was suggested as an unstructured structure from the IUPRED Web-server (<http://iupred.elte.hu/>) (*Dosztányi et al., 2005*) to predict disorder tendency. To calculate the distance between the GK domain and the inner surface of the PM, the WLC model was used. This model is usually used to describe the behavior of polymers that are semi-flexible: quite stiff with successive segments pointing in roughly the same direction, and with persistence length within a few orders of magnitude of the polymer length. This model is also used to describe unstructured proteins

like this linker structure (Zhou, 2001). In the WLC, the mean square end-to-end distance  $\langle R^2 \rangle$  is written as:

$$\langle R^2 \rangle = 2PL_0 \left[ 1 - \frac{P}{L_0} \exp\left(-\frac{L_0}{P}\right) \right]$$

where  $P$  is the polymer's characteristic persistence length and  $L_0$  is the maximum length. We used  $P = 0.6$  and  $L_0$  as  $(N - 1) \times 3.8$ , where  $N$  is number of amino acids in the unstructured protein (Lapidus et al., 2002). We then removed three amino acids in Lyn(MGC), which is directly connected to the membrane via palmitoylation and myristoylation. The root mean square end-to-end distance  $\sqrt{\langle R^2 \rangle}$ , which can be suggested as the average distance, was calculated.  $\sqrt{\langle R^2 \rangle}$  was 32.7 Å for six additional linkers, 36.0 Å for 11 aa, 38.4 Å for 15 aa, 42.4 Å for 22 aa, 52.5 Å for 43 aa, and 28.2 Å for no additional linker.

## Statistical analysis

Patch clamp data acquisition and analysis used Pulse/Pulse Fit 8.11 software with the EPC-10 patch clamp amplifier (HEKA Elektronik). Further data processing was performed with Igor Pro 6.2 (Wave-Metrics, Inc), Excel office 365 (Microsoft), and GraphPad Prism 7.0 (GraphPad Software, Inc). All quantitative data were presented as mean  $\pm$  standard error of the mean values. Comparisons between groups were analyzed by Student's two-tailed unpaired t-test. Comparisons among more than two groups were analyzed using one-way analysis of variance (ANOVA) followed by Tukey post hoc test. Comparisons among more than two groups with two independent variables were analyzed using two-way ANOVA followed by Sidak post hoc test. Differences were considered significant at the \* $p < 0.05$ , \*\* $p < 0.01$ , and \*\*\* $p < 0.001$ , as appropriate.

## Acknowledgements

We thank many laboratories for providing the plasmids.

## Additional information

### Funding


Funder	Grant reference number	Author
National Research Foundation of Korea	2020R1A6A3A01100500	Cheon-Gyu Park
National Research Foundation of Korea	2019R1A2B5B01070546	Byung-Chang Suh
National Research Foundation of Korea	2020R1A4A1019436	Byung-Chang Suh

The funders had no role in study design, data collection, and interpretation, or the decision to submit the work for publication.

### Author contributions

Cheon-Gyu Park, Conceptualization, Data curation, Formal analysis, Funding acquisition, Investigation, Visualization, Methodology, Writing - original draft; Wookyung Yu, Formal analysis; Byung-Chang Suh, Conceptualization, Resources, Supervision, Visualization, Project administration, Writing - review and editing

### Author ORCIDs

Cheon-Gyu Park  <http://orcid.org/0000-0002-4739-1913>  
 Wookyung Yu  <http://orcid.org/0000-0001-9835-930X>  
 Byung-Chang Suh  <http://orcid.org/0000-0003-0278-2459>

### Decision letter and Author response

Decision letter <https://doi.org/10.7554/eLife.69500.sa1>

Author response <https://doi.org/10.7554/eLife.69500.sa2>

## Additional files

### Supplementary files

- Supplementary file 1. Primers for  $\beta 2$  chimera constructs.
- Supplementary file 2. Primers for deletion or mutagenesis of  $\text{Ca}_v \alpha 1\text{B}$  and  $\beta 2$  constructs.
- Transparent reporting form

### Data availability

All data generated or analyzed during this study are included in the manuscript and supporting files.

## References

- Agler HL**, Evans J, Tay LH, Anderson MJ, Colecraft HM, Yue DT. 2005. G protein-gated inhibitory module of N-type ( $\text{Ca}_v 2.2$ )  $\text{Ca}^{2+}$  channels. *Neuron* **46**:891–904. DOI: <https://doi.org/10.1016/j.neuron.2005.05.011>, PMID: 15953418
- Banaszynski LA**, Liu CW, Wandless TJ. 2005. Characterization of the FKBP-rapamycin-FRB ternary complex. *Journal of the American Chemical Society* **127**:4715–4721. DOI: <https://doi.org/10.1021/ja043277y>, PMID: 15796538
- Berridge MJ**, Lipp P, Bootman MD. 2000. The versatility and universality of calcium signalling. *Nature Reviews. Molecular Cell Biology* **1**:11–21. DOI: <https://doi.org/10.1038/35036035>, PMID: 11413485
- Buraei Z**, Yang J. 2010. The  $\beta$  subunit of voltage-gated  $\text{Ca}^{2+}$  channels. *Physiological Reviews* **90**:1461–1506. DOI: <https://doi.org/10.1152/physrev.00057.2009>, PMID: 20959621
- Buraei Z**, Yang J. 2013. Structure and function of the  $\beta$  subunit of voltage-gated  $\text{Ca}^{2+}$  channels. *Biochimica et Biophysica Acta* **1828**:1530–1540. DOI: <https://doi.org/10.1016/j.bbamem.2012.08.028>, PMID: 22981275
- Catterall WA**. 2011. Voltage-Gated calcium channels. *Cold Spring Harbor Perspectives in Biology* **3**:a003947. DOI: <https://doi.org/10.1101/cshperspect.a003947>, PMID: 21746798
- Chen YH**, Li MH, Zhang Y, He LL, Yamada Y, Fitzmaurice A, Shen Y, Zhang H, Tong L, Yang J. 2004. Structural basis of the  $\alpha 1$ - $\beta$  subunit interaction of voltage-gated  $\text{Ca}^{2+}$  channels. *Nature* **429**:675–680. DOI: <https://doi.org/10.1038/nature02641>, PMID: 15170217
- Chen YH**, He LL, Buchanan DR, Zhang Y, Fitzmaurice A, Yang J. 2009. Functional dissection of the intramolecular src homology 3-guanylate kinase domain coupling in voltage-gated  $\text{Ca}^{2+}$  channel  $\beta$ -subunits. *FEBS Letters* **583**:1969–1975. DOI: <https://doi.org/10.1016/j.febslet.2009.05.001>, PMID: 19427861
- Chien AJ**, Carr KM, Shirokov RE, Rios E, Hosey MM. 1996. Identification of palmitoylation sites within the L-type calcium channel  $\beta 2\text{a}$  subunit and effects on channel function. *The Journal of Biological Chemistry* **271**:26465–26468. DOI: <https://doi.org/10.1074/jbc.271.43.26465>, PMID: 8900112
- Clapham DE**. 2007. Calcium signaling. *Cell* **131**:1047–1058. DOI: <https://doi.org/10.1016/j.cell.2007.11.028>, PMID: 18083096
- Dong Y**, Gao Y, Xu S, Wang Y, Yu Z, Li Y, Li B, Yuan T, Yang B, Zhang XC, Jiang D, Huang Z, Zhao Y. 2021. Closed-state inactivation and pore-blocker modulation mechanisms of human  $\text{Ca}_v 2.2$ . *Cell Reports* **37**:109931. DOI: <https://doi.org/10.1016/j.celrep.2021.109931>, PMID: 34731621
- Dosztányi Z**, Csizmok V, Tompa P, Simon I. 2005. IUPred: web server for the prediction of intrinsically unstructured regions of proteins based on estimated energy content. *Bioinformatics* **21**:3433–3434. DOI: <https://doi.org/10.1093/bioinformatics/bti541>, PMID: 15955779
- Felix R**. 2005. Molecular regulation of voltage-gated  $\text{Ca}^{2+}$  channels. *Journal of Receptor and Signal Transduction Research* **25**:57–71. DOI: <https://doi.org/10.1081/rrs-200068102>, PMID: 16149767
- Gao S**, Yao X, Yan N. 2021. Structure of human  $\text{Ca}_v 2.2$  channel blocked by the painkiller ziconotide. *Nature* **596**:143–147. DOI: <https://doi.org/10.1038/s41586-021-03699-6>, PMID: 34234349
- Heneghan JF**, Mitra-Ganguli T, Stanish LF, Liu L, Zhao R, Rittenhouse AR. 2009. The  $\text{Ca}^{2+}$  channel  $\beta$  subunit determines whether stimulation of Gq-coupled receptors enhances or inhibits N current. *Journal of General Physiology* **134**:369–384. DOI: <https://doi.org/10.1085/jgp.200910203>, PMID: 19858357
- Hille B**, Dickson EJ, Kruse M, Vivas O, Suh BC. 2015. Phosphoinositides regulate ion channels. *Biochimica et Biophysica Acta (BBA) - Molecular and Cell Biology of Lipids* **1851**:844–856. DOI: <https://doi.org/10.1016/j.bbalip.2014.09.010>, PMID: 25241941
- Huang J**, Zamponi GW. 2017. Regulation of voltage gated calcium channels by GPCRs and post-translational modification. *Current Opinion in Pharmacology* **32**:1–8. DOI: <https://doi.org/10.1016/j.coph.2016.10.001>, PMID: 27768908
- Hurley JH**, Cahill AL, Currie KPM, Fox AP. 2000. The role of dynamic palmitoylation in  $\text{Ca}^{2+}$  channel inactivation. *PNAS* **97**:9293–9298. DOI: <https://doi.org/10.1073/pnas.160589697>, PMID: 10900273
- Inoue T**, Heo WD, Grimley JS, Wandless TJ, Meyer T. 2005. An inducible translocation strategy to rapidly activate and inhibit small gtpase signaling pathways. *Nature Methods* **2**:415–418. DOI: <https://doi.org/10.1038/nmeth763>, PMID: 15908919
- Jeong JY**, Yim HS, Ryu JY, Lee HS, Lee JH, Seen DS, Kang SG. 2012. One-Step sequence- and ligation-independent cloning as a rapid and versatile cloning method for functional genomics studies. *Applied and Environmental Microbiology* **78**:5440–5443. DOI: <https://doi.org/10.1128/AEM.00844-12>, PMID: 22610439

- Jeong JY**, Kweon HJ, Suh BC. 2016. Dual regulation of R-type CaV2.3 channels by M1 muscarinic receptors. *Molecules and Cells* **39**:322–329. DOI: <https://doi.org/10.14348/molcells.2016.2292>, PMID: 26923189
- Kaur G**, Pinggera A, Ortner NJ, Lieb A, Sinnegger-Brauns MJ, Yarov-Yarovoy V, Obermair GJ, Flucher BE, Striessnig J. 2015. A polybasic plasma membrane binding motif in the I-II linker stabilizes voltage-gated Cav1.2 calcium channel function. *The Journal of Biological Chemistry* **290**:21086–21100. DOI: <https://doi.org/10.1074/jbc.M115.645671>, PMID: 26100638
- Keum D**, Baek C, Kim DI, Kweon HJ, Suh BC. 2014. Voltage-Dependent regulation of CaV2.2 channels by Gq-coupled receptor is facilitated by membrane-localized  $\beta$  subunit. *The Journal of General Physiology* **144**:297–309. DOI: <https://doi.org/10.1085/jgp.201411245>, PMID: 25225550
- Kim DI**, Kang M, Kim S, Lee J, Park Y, Chang I, Suh BC. 2015a. Molecular basis of the membrane interaction of the  $\beta$ 2e subunit of voltage-gated ca (2+) channels. *Biophysical Journal* **109**:922–935. DOI: <https://doi.org/10.1016/j.bpj.2015.07.040>, PMID: 26331250
- Kim DI**, Park Y, Jang DJ, Suh BC. 2015b. Dynamic phospholipid interaction of  $\beta$ 2e subunit regulates the gating of voltage-gated ca2+ channels. *The Journal of General Physiology* **145**:529–541. DOI: <https://doi.org/10.1085/jgp.201411349>, PMID: 25964431
- Kim D**, Kweon H, Park Y, Jang D, Suh BC. 2016. Ca<sup>2+</sup> controls gating of voltage-gated calcium channels by releasing the  $\beta$ 2e subunit from the plasma membrane. *Science Signaling* **9**:1–14. DOI: <https://doi.org/10.1126/scisignal.aad7247>
- Lapidus LJ**, Steinbach PJ, Eaton WA, Szabo A, Hofrichter J. 2002. Effects of chain stiffness on the dynamics of loop formation in polypeptides. Appendix: Testing a 1-dimensional diffusion model for peptide dynamics. *The Journal of Physical Chemistry B* **106**:11628–11640. DOI: <https://doi.org/10.1021/jp020829v>
- Li B**, Tadross MR, Tsien RW. 2016. Sequential ionic and conformational signaling by calcium channels drives neuronal gene expression. *Science* **351**:863–867. DOI: <https://doi.org/10.1126/science.aad3647>, PMID: 26912895
- Miranda-Laferte E**, Schmidt S, Jara AC, Neely A, Hidalgo P. 2012. A short polybasic segment between the two conserved domains of the  $\beta$ 2a-subunit modulates the rate of inactivation of R-type calcium channel. *The Journal of Biological Chemistry* **287**:32588–32597. DOI: <https://doi.org/10.1074/jbc.M112.362509>, PMID: 22851179
- Mitra-Ganguli T**, Vitko I, Perez-Reyes E, Rittenhouse AR. 2009. Orientation of palmitoylated cavbeta2a relative to Cav2.2 is critical for slow pathway modulation of N-type Ca2+ current by tachykinin receptor activation. *The Journal of General Physiology* **134**:385–396. DOI: <https://doi.org/10.1085/jgp.200910204>, PMID: 19858358
- Murata Y**, Iwasaki H, Sasaki M, Inaba K, Okamura Y. 2005. Phosphoinositide phosphatase activity coupled to an intrinsic voltage sensor. *Nature* **435**:1239–1243. DOI: <https://doi.org/10.1038/nature03650>, PMID: 15902207
- Okamura Y**, Murata Y, Iwasaki H. 2009. Voltage-Sensing phosphatase: actions and potentials. *The Journal of Physiology* **587**:513–520. DOI: <https://doi.org/10.1113/jphysiol.2008.163097>, PMID: 19074969
- Olcese R**, Qin N, Schneider T, Neely A, Wei X, Stefani E, Birnbaumer L. 1994. The amino terminus of a calcium channel beta subunit sets rates of channel inactivation independently of the subunit's effect on activation. *Neuron* **13**:1433–1438. DOI: [https://doi.org/10.1016/0896-6273\(94\)90428-6](https://doi.org/10.1016/0896-6273(94)90428-6), PMID: 7993634
- Opatowsky Y**, Chen CC, Campbell KP, Hirsch JA. 2004. Structural analysis of the voltage-dependent calcium channel beta subunit functional core and its complex with the alpha 1 interaction domain. *Neuron* **42**:387–399. DOI: [https://doi.org/10.1016/s0896-6273\(04\)00250-8](https://doi.org/10.1016/s0896-6273(04)00250-8), PMID: 15134636
- Park CG**, Park Y, Suh BC. 2017. The hook region of voltage-gated Ca2+ channel  $\beta$  subunits senses and transmits PIP2 signals to the gate. *The Journal of General Physiology* **149**:261–276. DOI: <https://doi.org/10.1085/jgp.201611677>, PMID: 28087621
- Park CG**, Suh BC. 2017. The hook region of  $\beta$  subunits controls gating of voltage-gated ca2+ channels by electrostatically interacting with plasma membrane. *Channels* **11**:467–475. DOI: <https://doi.org/10.1080/19336950.2017.1335841>, PMID: 28569643
- Qin N**, Platano D, Olcese R, Costantin JL, Stefani E, Birnbaumer L. 1998. Unique regulatory properties of the type 2A ca2+ channel beta subunit caused by palmitoylation. *PNAS* **95**:4690–4695. DOI: <https://doi.org/10.1073/pnas.95.8.4690>, PMID: 9539800
- Resh MD**. 1994. Myristylation and palmitoylation of Src family members: the fats of the matter. *Cell* **76**:411–413. DOI: [https://doi.org/10.1016/0092-8674\(94\)90104-x](https://doi.org/10.1016/0092-8674(94)90104-x), PMID: 8313462
- Richards MW**, Leroy J, Pratt WS, Dolphin AC. 2007. The HOOK-domain between the SH3 and the GK domains of cavbeta subunits contains key determinants controlling calcium channel inactivation. *Channels* **1**:92–101. DOI: <https://doi.org/10.4161/chan.4145>, PMID: 18690022
- Roberts-Crowley ML**, Rittenhouse AR. 2009. Arachidonic acid inhibition of L-type calcium (cav1.3b) channels varies with accessory cavbeta subunits. *The Journal of General Physiology* **133**:387–403. DOI: <https://doi.org/10.1085/jgp.200810047>, PMID: 19332620
- Rodríguez-Menchaca AA**, Adney SK, Zhou L, Logothetis DE. 2012. Dual regulation of voltage-sensitive ion channels by PIP (2). *Frontiers in Pharmacology* **3**:170. DOI: <https://doi.org/10.3389/fphar.2012.00170>, PMID: 23055973
- Subramanyam P**, Colecraft HM. 2015. Ion channel engineering: perspectives and strategies. *Journal of Molecular Biology* **427**:190–204. DOI: <https://doi.org/10.1016/j.jmb.2014.09.001>, PMID: 25205552
- Suh BC**, Inoue T, Meyer T, Hille B. 2006. Rapid chemically induced changes of PtdIns (4,5) P2 gate KCNQ ion channels. *Science* **314**:1454–1457. DOI: <https://doi.org/10.1126/science.1131163>, PMID: 16990515
- Suh BC**, Hille B. 2008. Pip2 is a necessary cofactor for ion channel function: how and why? *Annual Review of Biophysics* **37**:175–195. DOI: <https://doi.org/10.1146/annurev.biophys.37.032807.125859>, PMID: 18573078

- Suh BC**, Leal K, Hille B. 2010. Modulation of high-voltage activated Ca (2+) channels by membrane phosphatidylinositol 4,5-bisphosphate. *Neuron* **67**:224–238. DOI: <https://doi.org/10.1016/j.neuron.2010.07.001>, PMID: 20670831
- Suh BC**, Kim DI, Falkenburger BH, Hille B. 2012. Membrane-localized  $\beta$ -subunits alter the PIP2 regulation of high-voltage activated ca2+ channels. *PNAS* **109**:3161–3166. DOI: <https://doi.org/10.1073/pnas.1121434109>, PMID: 22308488
- Takahashi SX**, Mittman S, Colecraft HM. 2003. Distinctive modulatory effects of five human auxiliary beta2 subunit splice variants on L-type calcium channel gating. *Biophysical Journal* **84**:3007–3021. DOI: [https://doi.org/10.1016/S0006-3495\(03\)70027-7](https://doi.org/10.1016/S0006-3495(03)70027-7), PMID: 12719232
- Van Petegem F**, Clark KA, Chatelain FC, Minor DL. 2004. Structure of a complex between a voltage-gated calcium channel beta-subunit and an alpha-subunit domain. *Nature* **429**:671–675. DOI: <https://doi.org/10.1038/nature02588>, PMID: 15141227
- Wu L**, Bauer CS, Zhen XG, Xie C, Yang J. 2002. Dual regulation of voltage-gated calcium channels by ptdins (4,5) P2. *Nature* **419**:947–952. DOI: <https://doi.org/10.1038/nature01118>, PMID: 12410316
- Xie B**, Nguyen PM, Guček A, Thonig A, Barg S, Idevall-Hagren O. 2016. Plasma membrane phosphatidylinositol 4,5-bisphosphate regulates Ca (2+) -influx and insulin secretion from pancreatic  $\beta$  cells. *Cell Chemical Biology* **23**:816–826. DOI: <https://doi.org/10.1016/j.chembiol.2016.06.009>, PMID: 27447049
- Yang T**, He LL, Chen M, Fang K, Colecraft HM. 2013. Bio-inspired voltage-dependent calcium channel blockers. *Nature Communications* **4**:14950–14957. DOI: <https://doi.org/10.1038/ncomms3540>
- Yeon JH**, Park CG, Hille B, Suh BC. 2018. Translocatable voltage-gated ca2+ channel  $\beta$  subunits in  $\alpha$ 1- $\beta$  complexes reveal competitive replacement yet no spontaneous dissociation. *PNAS* **115**:E9934–E9943. DOI: <https://doi.org/10.1073/pnas.1809762115>, PMID: 30257950
- Zhou H-X**. 2001. Loops in proteins can be modeled as worm-like chains. *The Journal of Physical Chemistry B* **105**:6763–6766. DOI: <https://doi.org/10.1021/jp011355n>